NEW FRONTIERS IN CHEMISTRY
New Front. Chem.

(*former Annals of West University of Timișoara – Series of Chemistry*)

(2020) Volume 29, Number (Issue) 2, pp. 53-108

Ordinary Issue

TABLE OF CONTENTS

Opening of The Epoxide Ring. X-Ray Crystal Structure of The Opened Species and Identification of The Transition State by DFT **53-60**
Nirmal K. Shee, Shanti G. Patra, Michael G. B. Drew, and Dipankar Datta
Modeling Copper Nanoparticles as Catalysts for the Oxygen Reduction Reaction in Fuel Cells **61-67**
Frank J. Owens
Topo-chemical reactivity study on molecular machines **69-97**
Nicoleta A. Dudaş, Ottorino Ori, and Mihai V. Putz
Chemometrics Study of Germs Plant for Determining Anticancer Activity **99-108**
Alina-Maria Petrescu, Lauriana–Eunice Zbîrcea, Maria-Roxana Buzan, Gianina Loredana Jucos, Feng Chen Ifrim, Gheorghe Ilia, Virgil Paunescu

PUBLISHER:
Universitatea de Vest
din Timişoara

NEW FRONTIERS IN CHEMISTRY: METADATA

New Frontiers in Chemistry (New Front. Chem.) is an open-access fee-free peer-review international academic journal addressing the modern trends and frontiers in fundamental, applicative and multidisciplinary chemistry, paralleling the ever-expanding chemical data, methods, and compounds available and continuously produced, towards cross fertilizing the multidisciplinary ideas as coming from Chemistry combined with Mathematics, the Natural and Applied sciences (Physics, Biology, Medicine, Agriculture, Environmental, Engineering), and beyond.

NEW FRONTIERS IN CHEMISTRY
(NEW FRONT. CHEM.)
is published biannually by

West University of Timișoara
Blvd. V. Parvan 4
Timisoara 300223, ROMANIA
E-mail: newfrontchem@iqstorm.ro
Web: www.newfrontchem.iqstorm.ro

ISSN 2668-9189
ISSN-L 2393 – 2171

Subscription Price per Volume
Electronic: open access   Print: on demand by above email address

Additional color graphics is available in the e-version of this Journal

NEW FRONTIERS IN CHEMISTRY: EDITORS

Editorial Board:

Advisory Editors

(from active members of Biology-Chemistry Department and of Doctoral School of Chemistry of West University of Timișoara):

VASILE OSTAFE (Biochemistry, Chromatography, Environmental Chemistry)
IONEL CIUCANU (Instrumental Techniques for Analytical Chemistry)
ADRIANA ISVORAN (Biophysics, Bioinformatics)
MIHAI V. PUTZ (Nanochemistry, Quantum Chemistry)
TITUS VLASE (Thermal Analysis, Chemical Kinetics, Chemistry of Solid State)
GABRIELA VLASE (Inorganic Chemistry, Thermal Analysis)
GABRIELA PREDA (Organic Chemistry, Catalysis)
CONSTANTIN BOLCU (Organic Chemistry, Polymers)
VLAD CHIRIAC (General and Analytical Chemistry, Electrochemistry)
DANA VLASCICI (Analytical Chemistry)
DANIELA DASCALU (Thermodynamics and Chemical Statistics)
CORINA DUDA-SEIMAN (QSAR, Organic Chemistry, Medicinal Chemistry)
LAURA PITULICE (Environmental Chemistry)
BEATRICE VLAD-OROS (Chemical and Enzyme Kinetics)
NICOLETA IANOVIC (Aerobiology, Plant Physiology)

Honorary Editors

(as Doctor Honoris Causa of WUT/CBG & Formers Editors and Developers of Annals of West University of Timișoara – Series Chem.):

ALEXANDRU BALABAN (Texas A&M University at Galveston, USA, & Romanian Academy, Romania)
HAGEN KLEINERT (Berlin Free University, Germany)
KATLEEN SWALLOW (Merrimack College, USA)
GABOR NÁRÁY-SZABÓ ("Lorand Eőtvős" University Budapest, Hungary)
MARIUS ANDRUH (Romanian Academy, Bucharest)
VASILE OSTAFE (West University of Timisoara, Romania)
VICTOR EMANUEL SAHINI (†, Polytechnic Bucharest, Romanian Academy, Romania)
EUGEN SEGAL (†,University of Bucharest, Romanian Academy, Romania)
ZENO SIMON (†, Romanian Academy, Romania)
ADRIAN CHIRIAC (†, West University of Timisoara, Romania)
MIRCEA MRACEC (†, West University of Timisoara, Romania)
NICOLAE BONCIOCAT (†, Babes-Bolyai University, Cluj-Napoca, Romania)
ALAN R. KATRITZKY (†, University of Florida, Gainesville, USA)

NEW FRONT. CHEM. (2020)
Volume 29, Number 2, pp. 53-60
ISSN 2668-9189; ISSN-L 2393-2171

Former: Ann. West Univ. Timisoara – Series Chem.
ISSN: 1224-9513

Article

OPENING OF THE EPOXIDE RING. X-RAY CRYSTAL STRUCTURE OF THE OPENED SPECIES AND IDENTIFICATION OF THE TRANSITION STATE BY DFT

Nirmal K. Shee,[1] Shanti G. Patra,[1] Michael G. B. Drew[2], and Dipankar Datta[1]♣

[1] Department of Inorganic Chemistry, Indian Association for the Cultivation of Science, Calcutta 700 032, India
[2] Department of Chemistry, University of Reading, Whiteknights, Reading RG6 6AD, UK

ABSTRACT

Ring-opening of oxiranes by nucleophiles is very important in chemical synthesis. But these reactions are limited by slow reaction rate, poor yield, use of high temperature and Lewis acid catalyst. Reaction of 5,6-dihydro-5,6-epoxy-1,10-phenanthroline (L) with 4-methylaniline produces L', a 2-amino alcohol. Good yield has been obtained in water medium at room temperature without using any Lewis acid catalyst. The product crystallizes in the space group $P2_1/a$ as L'.H_2O with $Z = 4$. X-ray crystal structure shows that the water molecule acts as a donor of two H-bonds to the phenanthroline N atoms as well as an acceptor of two H-bonds from the N-H moiety of two L'. The transition state (TS) has been located at the B3LYP/6-31+G(d,p) level. The free energy of activation is estimated as 48.76 kcal mol^{-1} in gas phase. It decreases significantly to 34.79 kcal mol^{-1} when solvation is considered revealing the role of water in the reaction.

Keywords: epoxide, epoxide opening, X-ray crystal structure, DFT, transition state

---

♣ Correspondent author: icdd@iacs.res.in

1. INTRODUCTION

2-Amino alcohols are important versatile intermediates in the synthesis of numerous biologically active natural compounds, chiral auxiliaries, and amino acids [1-3]. These have considerable use in medicinal chemistry [4,5]. Generally, opening of the 3-membered heterocyclic strained epoxide ring by amines leads to the formation of 2-amino alcohols. However, there are some limitations of this approach such as slow reaction rate, poor yield, poor sensitivity of epoxides, need of excess of nucleophiles and often high temperature, weak nucleophilic character of amines, and regio-selective nature of the compounds [6]. In nature, phenolic proton of a tyrosine moiety catalyses the ring opening of oxiranes in water [7].

Researchers have been using a variety of Lewis acid catalysts such as alumina, metal amides, and metal triflates that can enhance the electrophilic character of epoxides [8-10]. There are some reports where use of a catalyst has not been necessary [11,12]. Hydrogen bonding interaction, hydrophobic interaction, and solvent polarity are the main factors that influence the selectivity and reactivity of the process. Recently, we have undertaken a program to develop the transition metal chemistry of 5,6-dihydro-5,6-epoxy-1,10-phenanthroline (L). We have synthesized its tris complexes of Fe, Ni, Cu and Zn [13-16]. The epoxide ring in the metal chelates is found to be very much susceptible to nucleophilic attack. Other workers have also tried to open up the epoxide ring in L [17-19]. Previously, we have found that simple stirring of ML_3 (M: a metal) with 4-substituted anilines in equimolar proportion in water at room temperature without any Lewis acid catalyst gives high yield of chelated 2-amino alcohols [14,15]. We have determined the X-ray crystal structures of ML_3. But could not determine the structure of the ring opened species. Here we present the X-ray crystal structure of L' where the epoxide ring in L has been opened by 4-methylaniline (Scheme I). So far X-ray crystal structure of no compounds having opened epoxide ring has been reported.

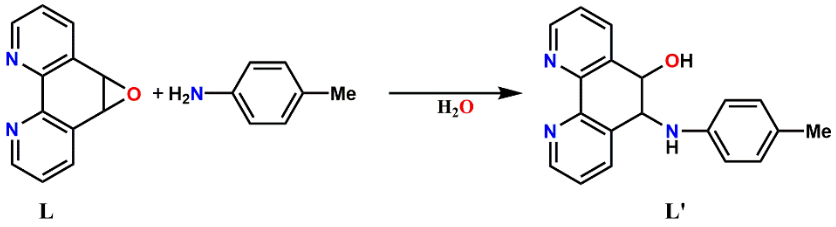

Scheme I. Opening of the epoxide ring in L by 4-methylaniline

2. RESULTS & DISCUSSIONS

Simple stirring of L with 4-methylaniline at room temperature in water in equimolar proportion affords $L'.H_2O$ in 90% yield. We have obtained the single crystals of $L'.H_2O$ from *n*-hexane-dichloromethane mixture. Its X-ray crystal structure is shown in Figure 1. Selected crystal data are given in Table 1.

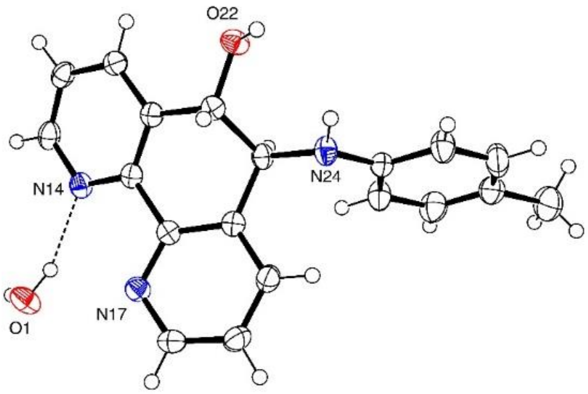

Figure 1. The X-ray crystal structure of L'.H_2O with ellipsoids at 30% probability. H-bond is shown as dotted line.

Table 1. Some crystal and structure refinement data for L'.H_2O

Empirical formula	$C_{19}H_{19}N_3O_2$
Formula weight	321.37
Crystal system	Monoclinic
Space group	$P2_1/a$
Cell dimensions	
a (Å)	17.146(9)
b (Å)	4.8782(10)
c (Å)	20.999(8)
β (deg)	110.94(5)
V (Å^3)	1640.4(11)
Z	4
D_{calcd} (g cm^{-3})	1.301
μ (mm^{-1})	0.086
F (000)	680
θ_{max} (deg)	30
Unique reflections	4538
Observed reflections $[I > 2\sigma(I)]$	3007
Parameters	230
GOF on F^2	0.970
R_1, wR_2 $[I > 2\sigma(I)]$	0.0600, 0.1331
R_1, wR_2 (all data)	0.0947, 0.1532
Largest peak/hole (e Å^{-3})	0.316/-0.216

The water molecule O(1) participates in four strong hydrogen bonds, acting twice as a donor to N(17) and N(14) and twice as an acceptor from N(24) and O(22). Thus, all four heteroatoms in the molecule participate in hydrogen bonding. Hydrogen bond dimensions are given in Table 2.

Table 2. Hydrogen bonds in L'.H_2O (distances, Å; angles, deg; A = acceptor, D = donor). For atom labelling, see Figure 1.

	H…A	D…A	D-H…A	symmetry operation
N(24)-H24… O(1)	2.21(2)	3.066(3)	163(2)	x-1/2, 1.5-y, z
O(1)-H(1)… N(14)	2.02(2)	2.856(3)	161(2)	
O(1)-H(2)… O(22)	1.93(2)	2.769(2)	176(2)	1/2+x, 2.5-y,z
O(22)-H(22)…O(1)	1.88(2)	2.674(2)	156(2)	x-1/2, 1.5-y,z

Opening of the epoxide ring by an amine is a typical nucleophilic reaction. We have studied the reaction by density functional theory (DFT) at the B3LYP/6-31+G(d,p) level. Here a new C-N bond is formed, and an existing C-O bond is broken as the reaction proceeds from the reactants to product. A shortening of C-N bond and lengthening of C-O bond are observed along the reaction path. The transition state (TS) is pictorially shown in Figure 2. It has a single imaginary frequency (335.52*i*). Some bond length and angles for the TS and the product are compared in Table 3. The free energy of activation is found to be 48.76 kcal mol^{-1} in gas phase. However, when solvation energy in water is considered, the free energy of activation is reduced to 34.79 kcal mol^{-1} which is comparable to the other reported values [20]. The barrier is low enough to permit a smooth reaction between L and 4-methylaniline at room temperature in aqueous medium.

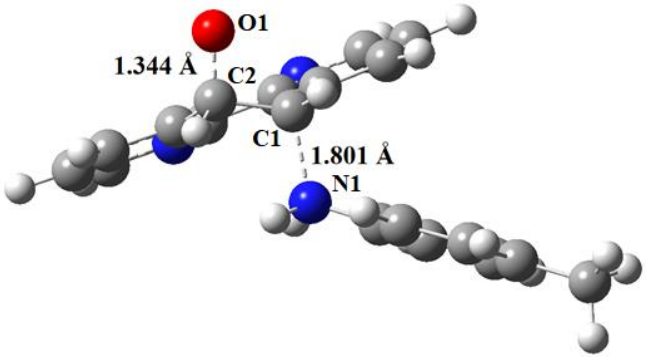

Figure 2. DFT structure of the transition state showing the C-O and C-N bond lengths. Color code: white, H; grey, C; blue, N and red, O.

Table 3. Data of some bond lengths (Å), bond angles (°) and a torsion angle (°) in the transition state and the final product at the B3LYP/6-31+G(d,p) level. For atom labelling, see Figure 2.

metric parameter	transition state	product
N1-C1	1.801	1.456
C1-C2	1.516	1.546
C1-O1	2.197	2.463
C2-O1	1.344	1.420
N1-C1-C2	108.29	112.13
O1-C2-C1	106.32	112.18
N1-C1-C2-O1	169.26	60.83

3. COMPUTATIONAL

All electronic structure calculations have been carried out using the Gaussian 09 program package [21]. The hybrid nonlocal density functional B3LYP and 6-31+G(d,p) basis set are employed for the calculation. The transition state is optimized using Berny algorithm as implemented in Gaussian 09. Conductor like polarization continuum model (CPCM) [22] has been used to calculate the solvation energy in water ($\varepsilon = 78.54$). Single point energies of the optimized geometries (gas phase) in aqueous medium are calculated to consider the solvation effect.

4. EXPERIMENTAL

4.1. Materials and physical measurements

L, 4-methylaniline were purchased from Aldrich. Micro-analyses were performed by a Perkin-Elmer 2400II elemental analyser. FTIR spectra (KBr) were recorded on a Shimadzu FTIR-8400S spectrometer, 300 MHz NMR spectra on a Bruker DPX300 spectrometer, and ESI mass spectra on a Waters Qtof Micro YA263 spectrometer.

4.2. Synthesis of L'.H_2O

Method A. L (0.039 g, 0.2 mmol) and 4-methylaniline (0.021 g, 0.2 mmol) were taken in water (50 ml) and stirred for 72 h. The white compound precipitated was collected by filtration, washed with water (2 ml) and dried in vacuo over fused $CaCl_2$. Yield: 0.055 g (90%). *Method B*. The reactants were refluxed for 14 h. Then the clear orangish solution was evaporated to 10 ml and cooled to room temperature. A yellowish compound so obtained was filtered off and dried in vacuo over fused $CaCl_2$. Yield: 0.037 g (60%). m. p. 239 ^{o}C. *Anal*. Calc. for $C_{19}H_{19}N_3O_2$: C, 70.99; H, 5.96; N, 13.07. Found: C, 70.81; H, 5.82; N, 13.10%. FTIR: ν/cm^{-1}: 3371vs (NH). ESI-MS (CH_3CN): m/z: 342.2 [(L' + K)$^+$, 100%]. ^{1}H NMR (DMSO-d$_6$): δ/ppm: 2.15 (s, 3H, methyl), 4.62 (t, 6 Hz, 1H, CHN), 4.84 (t, 6 Hz, 1H, CHO), 5.69 (d, 6 Hz, 1H, NH), 5.78 (d, 6 Hz, 1H, OH), 6.61 (d, 9 Hz, 2H, phenyl), 6.90 (d, 9 Hz, 2H phenyl), 7.40 (m, 2H, phen), 7.74 (d, 6 Hz, 1H, phen), 7.89 (d, 6 Hz, 1H, phen), 8.65 (t, 6 Hz, 2H, phen).

4.3. X-ray crystallography

4538 independent reflection data were collected with MoKα at 150K using the Oxford Diffraction X-Calibur CCD System. The crystals were positioned at 50 mm from the CCD and 321 frames were measured. Data analyses were carried out with the CrysAlis program [23]. The structure was solved using direct methods with the Shelxs97 program [24]. The non-hydrogen atoms were refined with anisotropic thermal parameters. The hydrogen atoms bonded to carbon were included in geometric positions and given thermal parameters equivalent to 1.2 times those of the atom to which they were attached. Hydrogen atoms bonded to nitrogen or oxygen were located in a difference Fourier map and refined with distance constraints. The structure was refined on F^2 using Shelxl97 [24].

5. CONCLUSIONS

It is concluded that L can undergo opening of the epoxide ring by 4-methyl aniline in water at room temperature in the absence of any Lewis acid catalyst to form L'.H_2O. The crystal structure of L'.H_2O shows presence of N-H…O and O-H…N type of hydrogen bonding. DFT calculations show breaking of a C-O bond formation of a C-N bond in the TS. The free energy of activation decreases significantly when solvation in water is considered proving the role of water in easing the reaction.

SUPPLEMENTARY MATERIALS AVAILABLE

CCDC-1936996 contains the supplementary crystal data for L'.H_2O. These data can be obtained free of charge from the Cambridge Crystallo-graphic Data Centre via w.w.w.ccdc.cam.ac.uk/data_request/cif.

ACKNOWLEDGEMENT

M.G.B.D. thanks EPSRC and the University of Reading for funds for the X-Calibur system.

REFERENCES

[1] J. Cossy, D. G. Pardo, C. Dumas, O. Mirguet, I. Déchamps, T. X. Métro, B. Burger, R. Roudeau, J. Appenzeller and A. Cochi, Rearrangement of beta-amino alcohols and application to the synthesis of biologically active compounds, *Chirality*, 2009, **21**, 850-856.

[2] F. Kudo, A. Miyanaga, T. Eguchi, Biosynthesis of natural products containing β-amino acids, ***Nat. Prod. Rep.*, 2014, 31**, 1056-1073,

[3] W. Chrisman. J. N. Camara, K. Marcellini, B. Singaram, C. T. Goralski, D. L. Hasha, P. R. Rudolf, L. W. Nicholson, K. K. Borodychuk, A simple and convenient synthesis

of β-amino alcohol chiral auxiliaries based on limonene oxide, *Tetrahedron Lett*., 2001, **42**, 5805-5807.

[4] F. D. Klingler, Asymmetric Hydrogenation of Prochiral Amino Ketones to Amino Alcohols for Pharmaceutical Use, *Acc. Chem. Res*., 2007, **40**, 1367-1376.

[5] K. Kopka, S. Wagner, B. Riemann, M. P. Law, C. Puke, S. K. Luthra, V. W. Pike, T. Wichter, W. Schmitz, O. Schober, M. Schäfers and M. Design of new β_1-selective adrenoceptor ligands as potential radioligands for in vivo imaging, *Bioorg. Med. Chem*., 2011, **11**, 3513-3527.

[6] F. A. Saddique, A. F. Zahoor, F. Sadia, S. A. R. Naqvi, M. Usman and M. Ahmad, Recent trends in ring opening of epoxides by amines as nucleophiles, *Synth. Commun*., 2016, **46**, 831-868.

[7] R. Rink, J. Kingma, J. H. L. Spelberg and D. B. Janssen, Tyrosine Residues Serve as Proton Donor in the Catalytic Mechanism of Epoxide Hydrolase from Agrobacterium radiobacter, *Biochem*., 2000, **39**, 5600-5613.

[8] G. H Posner and D. Z. Rogers, Organic reactions at alumina surfaces. Mild and selective opening of epoxides by alcohols, thiols, benzeneselenol, amines, and acetic acid, *J. Am. Chem. Soc*., 1077, **99**, 8208-8214.

[9] J. Cossy, V. Bellosta, C. Hamoir and J.-R. Desmurs, Regioselective ring opening of epoxides by nucleophiles mediated by lithium bistrifluoromethanesulfonimide, *Tetrahedron Lett*., 2002, **43**, 7083-7086.

[10] T. Ollevier and G. L. Compin, Bismuth triflate-catalyzed mild and efficient epoxide opening by aromatic amines under aqueous conditions, *Tetrahedron Lett*., 2004, **45**, 49-52.

[11] N. Azizi and M. R. Saidi, Highly Chemoselective Addition of Amines to Epoxides in Water, *Org. Lett*., 2005, **7**, 3649-365.

[12] C. Philippe, T. Milcent, B. Crousse and D. B. Delpon, Non Lewis acid catalysed epoxide ring opening with amino acid esters, *Org. Biomol. Chem*., 2009, **7**, 2026-2018.

[13] N. K. Shee, D. Das, F. A. O. Adekunle, M. G. B. Drew and D. Datta, Homoleptic copper (II) and copper (I) complexes of 5, 6-dihydro-5, 6-epoxy-1, 10-phenanthroline. Six-coordinate copper (I) in solution, *Inorg. Chim. Acta*, 2011, **366**, 198-202.

[14] N. K. Shee, F. A. O. Adekunle, D. Das, M. G. B. Drew and D. Datta, Epoxide ring opening in a zinc (II) complex in water without any Lewis acid catalyst: Formation of only one diastereomer out of 2^3, *Inorg. Chim. Acta*, 2011, **375**, 101-105.

[15] N. K. Shee, M. G. B. Drew and D. Datta, Ligand substituents effect on 10Dq, *Spectrochim. Acta Part A*, 2012, **97**, 1111-1114.

[16] N. K. Shee, M. G. B. Drew and D. Datta, Isolation of a metal-to-ligand charge-transfer (MLCT) state of a tris 1, 4-diimine complex of iron in the solid state: X-ray crystal structure and EPR, *New J. Chem*., 2017, **41**, 452-456.

[17] Y. Shen and B. P. Sullivan, Versatile Preparative Route to 5-Substituted-1,10-phenanthroline Ligands via 1,10-Phenanthroline-5,6-epoxide, *Inorg. Chem.*, 1995, **34**, 6235-6236.

[18] E. Schoffers, S. D. Tran and K. Mace, Preparation of Chiral 5,6-trans-Disubstituted Phenanthrolines From Phenanthroline-5,6-epoxide, *Heterocycles*, 2003, **60**, 769-772.

[19] S. Dwaraknath, N. H. Tran, T. Dao, A. Colbert, S. Mullen, A. Nguyen, A. Cortez, L. Cheruzel, A facile and versatile methodology for cysteine specific labeling of proteins with octahedral polypyridyl d^6 metal complexes, *J. Inorg. Biochem*., 2014, **136,** 154-160.

[20] J. -E. Ehlers, N. G. Rondan, L. K. Huynh, H. Pham, M. Marks and T.N. Truong, Theoretical Study on Mechanisms of the Epoxy-Amine Curing Reaction, Macromolecules, 2007, **40**, 4370-4377.

[21] M. J. Frisch, G. W. Trucks, H. B. Schlegel, G. E. Scuseria, M. A. Robb, J. R.Cheeseman, G. Scalmani, V. Barone, B. Mennucci, G. A. Petersson, H. Nakatsuji,M. Caricato, X. Li, H. P. Hratchian, A. F. Izmaylov, J. Bloino, G. Zheng, J. L.Sonnenberg, M. Hada, M. Ehara, K. Toyota, R. Fukuda, J. Hasegawa, M. Ishida, T. Nakajima, Y. Honda, O. Kitao, H. Nakai, T. Vreven, J. A. Montgomery, Jr., J. E. Peralta, F. Ogliaro, M. Bearpark, J. J. Heyd, E. Brothers, K. N. Kudin, V. N. Staroverov, T. Keith, R. Kobayashi, J. Normand, K. Raghavachari, A. Rendell, J. C. Burant, S. S. Iyengar, J. Tomasi, M. Cossi, N. Rega, J. M. Millam, M. Klene, J. E. Knox, J. B. Cross, V. Bakken, C. Adamo, J. Jaramillo, R. Gomperts, R. E. Stratmann, O. Yazyev, A. J. Austin, R. Cammi, C. Pomelli, J. W. Ochterski, R. L. Martin, K. Morokuma, V. G. Zakrzewski, G. A. Voth, P. Salvador, J. J. Dannenberg, S. Dapprich, A. D. Daniels, O. Farkas, J. B. Foresman, J. V. Ortiz, J. Cioslowski, D. J. Fox, GAUSSIAN09, Revision C.01, Gaussian, Inc., Wallingford, CT, 2010.

[22] M. Cossi, N. Rega, G. Scalmani and V. Barone, Energies, structures, and electronic properties of molecules in solution with the C-PCM solvation model, *J. Comput. Chem.*, 2003, **24**, 669-681.

[23] CrysAlis, Oxford Diffraction Ltd., Abingdon, U.K. 2006.

[24] G. M. Sheldrick, Shelxs97 and Shelxl97, Programs for Crystallographic solution and refinement, *ActaCrystallogr*. 2008, A64, 112─122.

NEW FRONT. CHEM. (2020)
Volume 29, Number 2, pp. 61-67
ISSN 2668-9189; ISSN-L 2393-2171
© West University of Timişoara

Former: Ann. West Univ. Timisoara – Series Chem.
ISSN: 1224-9513

Article

MODELING COPPER NANOPARTICLES AS CATALYSTS FOR THE OXYGEN REDUCTION REACTION IN FUEL CELLS

Frank J. Owens ♣
Dept. Physics, Hunter College of the City University of New York, 695 Park Ave. N.Y. 10065 N.Y (USA)

ABSTRACT

The dissociation of O_2 and HO_2 are important reactions that occur at the cathode of fuel cells producing H_2O and use platinum as a catalyst. There is a need to replace platinum with less expensive catalysts. Here the possibility of copper nanostructures as catalysts for the reactions is considered using density functional theory. The calculations employing density functional theory at the B3LYP/6-31G* level show that the bond dissociation energies to remove OH from O_2H bonded to copper nanostructures Cu_6,Cu_8,and Cu_{10} are significantly less than those necessary to dissociate free O_2H indicating that copper nanostructures could be catalysts for the dissociation of O_2H. However, the copper nanostructures are shown not to catalyze O_2 dissociation.

Keywords: copper nanostructures, Density Functional Theory, catalysis, oxygen reduction reaction.

1. INTRODUCTION

Presently platinum is employed to catalyze the reactions that produce H_2O at the cathode of fuel cells. Platinum is expensive and susceptible to time dependent drift and CO poisoning [1, 2]. These issues are significant obstacles to the development of large scale commercial application of fuel cells. Likely reactions that produce H_2O at the cathodes are the dissociation of O_2 bonded to the catalyst followed by atomic oxygen undergoing the following reaction,

$$2O + 4H^{+} + 4e \rightarrow 2H_2O \qquad (1)$$

♣ Correspondence: owensfj@gmail.com

Another possibility is the formation of O_2H which bonds to the catalyst followed by the removal of OH which could then undergo the following reaction,

$$OH + H^+ + e \rightarrow H_2O \tag{2}$$

For the catalyst to be effective the energy needed to dissociate O and OH from O_2 and O_2H bonded to the catalyst should be significantly lower than that required to dissociate free O_2 and O_2H. The traditional approach to developing new catalysts is to identify a candidate based on the know properties of a material. The material is then synthesized and tested by such methods as cyclic voltammetry. Such an approach is time consuming and does not always lead to the best catalyst. Theoretical modeling of catalysts has the potential to provide a rapid, reliable and a less costly method to identify new catalysts. Further it can often identify the details of the reaction which is not always possible from the cyclic voltammetry measurement. Modeling has been used to understand the role of platinum as a catalyst in fuel cells [3]. It also has been employed to predict possible potential new catalysts. For example molecular orbital theory has been used to predict that boron nitride nanoribbons as well as nitrogen doped graphene could be effective catalysts for reactions at the cathode of fuel cells [4, 5, 6].

2. METHODS

The minimum energy structures of Cu_NO_2, Cu_NO, and Cu_NO_2H, where Cu_N is a copper nanostructure ,are calculated using DFT at the B3LYP/6-31G* level employing Gaussian software.[7] The frequencies of the structures are calculated to insure the absence of imaginary frequencies which indicates the obtained structures are at a minimum on the potential energy surface. To determine if the copper nanoparticles can catalyze the production of O and OH from O_2 and O_2H bonded to Cu_N, nanoparticles the bond dissociation energy (BDE), to remove O and OH from these structures is calculated.

$$BDE = \left[E\left(Cu_NO\right) + E\left(OH\right)\right] - \left[E\left(Cu_NO_2H\right)\right] \tag{3}$$

where E is the total electronic energy plus the zero point energy (ZPE) of the minimum energy structure. The ZPE is the total ZPE of all of the normal modes of vibration given by,

$$E_{zpe} = \left(1/2\right)h\sum_{i}^{3N-6} f_i \tag{4}$$

where f_I are the vibrational frequencies of the normal modes and N the number of atoms in the molecule. An analogous expression is used for the dissociation of O_2. The calculated BDE given by equation 3 is compared with that to dissociate free O_2 or O_2H. If it is significantly less, it can be concluded that Cu_N is a good potential catalyst for the dissociation of O_2 and O_2H. Bond dissociation energies calculated by DFT have been show to be in reasonably good agreement with experimentally measured activation energy values [8, 9].

Another issue that needs to be considered in assessing whether copper nano-structures catalyze the reactions at the cathode is whether O_2 or O_2H can bond to the structures. This can be evaluated by calculating the adsorption energy, E_{ade}, given by [10],

$$E_{ade} = E\left(Cu_NO_2H\right) - E\left(Cu_N\right) + E\left(O_2H\right) \tag{5}$$

where E is the total electronic energy of the system at the minimum energy structure. If the result is a negative value, it indicates O_2 or O_2H can form a stable bond with the copper nanostructures.

3. RESULTS

Figures 1, 2 and 3 show the calculated minimum energy structure of O_2H, O_2 and O bonded to a Cu_6 nanoparticle. The structures have no imaginary frequencies indicating they are at a minimum on the potential energy surface. The calculated BDE to remove O from O_2 bonded to Cu_6 is 5.5eV which is slightly greater than that needed to dissociate free O_2. This indicates that Cu_6 would not be a catalyst to dissociate O_2. It turns out this is also true of the larger Cu nanostructures Cu_8 and Cu_{10} considered.

Figure 1: Minimum energy structure of O_2H bonded to a Cu_6 copper particle.

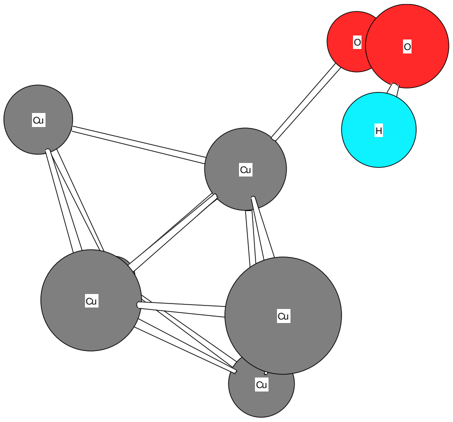

Figure 2: Minimum energy structure of O_2H bonded to a Cu_6 copper particle.

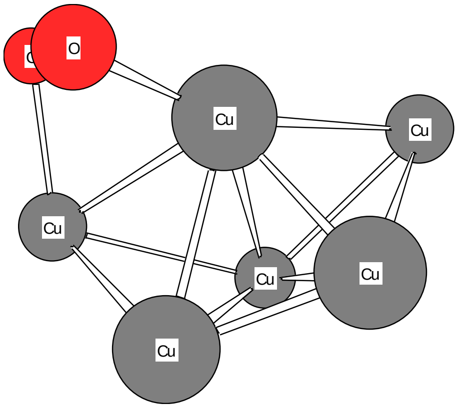

Figure 3: Minimum energy structure of an O atom bonded to Cu_6.

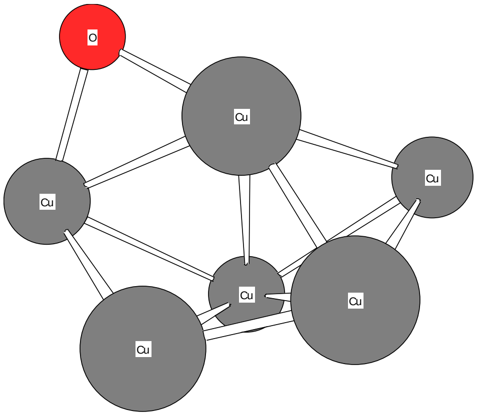

Thus the remainder of the paper will focus on O_2H dissociation. The calculated BDE to remove OH from O_2H bonded to Cu_6 is 0.21 eV, much smaller than that needed to dissociate free O_2H which is calculated to be 5.0 eV. This indicates that Cu_6 could be an effective catalyst for removing OH from O_2H. The calculated BDEs for removal of OH from O_2H bonded to all the structures considered are given in Table I. The calculated ades for O_2H to bond to all the Cu nanoparticles considered are given in Table II and are negative indicating that O_2H can bond to all the structures.

Table 1: Calculated bond dissociation energy to remove OH from O_2H bonded to Cu_N nanoparticles.

Particle type	Bond dissociation energy (eV)
Cu_{10}	0.42
Cu_8	0.61
Cu_6	0.21

Table 2: Calculated adsorption energy for O_2H to bond to Cu_N nanoparticles.

Particle Type	Adsorption Energy (eV)
Cu_{10}	-3.5
Cu_8	-3.7
Cu_6	-1.9

Figure 4 shows the minimum energy structure of O_2H bonded to Cu_8. Figure 5 is O bonded to Cu_8. The structures have no imaginary frequencies. The calculated ade given in Table II is negative indicating that O_2H can bond to Cu_8. The calculated BDE to remove OH from the structure is 0.61 eV suggesting that Cu_8 could also be a catalyst for O_2H dissociation. Figure 6 shows the calculated minimum energy structure of O_2H bonded to Cu_{10}. Figure 7 is the calculated structure of O bonded to Cu_{10}. The calculated ade given in table II is negative showing that O_2H can bond to Cu_{10}. The calculated BDE to remove OH from Cu_{10} is 0.42eV suggesting that this structure can also be a good catalyst for O_2H dissociation.

Figure 4: Minimum energy structure of O_2H bonded to a Cu_8 nanoparticle

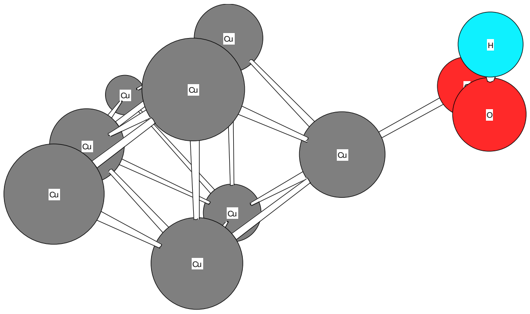

Figure 5: Minimum energy structure of an oxygen atom bonded to Cu_8

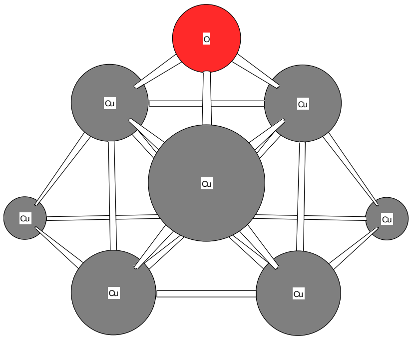

Figure 6: Minimum energy structure of O_2H bonded to Cu_{10}

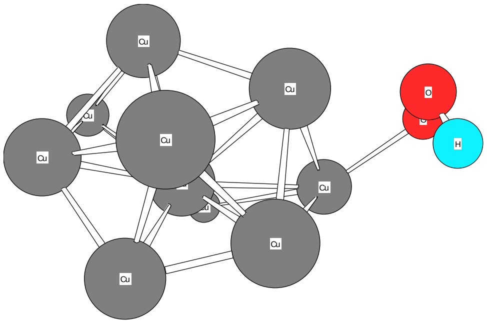

Figure 7: Minimum energy structure of an O atom bonded to Cu_{10}

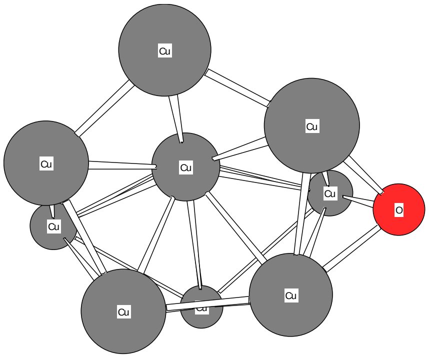

Stability of Cu_NO_2H structures

It is also necessary that the O_2H bonded to the copper nanostructures be thermally stable over the usable temperature range of a fuel cell which for a polymer electrolyte membrane (PEM) fuel cell is 50 ^{0}C to 100 ^{0}C. The calculated BDEs to remove O_2H from the copper nanostructures, given in Table III, are all large enough to suggest the structures are thermally stable over the usable temperature range of PEM fuel cell.

Table 3: Calculated bond dissociation energy to remove O_2H from copper particles

Particle type	Bond dissociation energy (eV)
Cu_{10}	3.1
Cu_8	3.2
Cu_6	2.0

*The bond lengths of the structures shown below will be provided on request.

4. CONCLUSION

The model used here based on bond dissociation energies calculated by DFT at the B3LYP/6-31G* level has been shown to predict catalytic activity in small copper nanoparticles. The minimum energy structure of O, O_2 and O_2H bonded to Cu_6, Cu_8, and Cu_{10} have been calculated by density functional theory. The bond dissociation energy to remove OH from O_2H bonded to the structures was quite low, less than 0. 61 eV suggesting that these structures could be catalysts for this ORR reaction. However, the structures were not indicated to be catalysts for O_2 dissociation. The calculations indicate that O_2H bonded to the structures should be stable over the operating temperature range of a PEM fuel cell. Interestingly there have been some experimental observations that copper nanostructures can be catalysts for the ORR reaction lending support to the theoretical approach employed [11].

REFERENCES

1. Yu, X.; Ye, S. Recent Advances in activity and durability enhancement of catalytic electrodes in PEMFC. *Journal of Power Sources* **2007**, *172*, 145-154.
2. Winter, M.; Brood, R.J. What are batteries, fuel cells and supercapicators. *Chemical Reviews* **2004**, *104*, 4245-4270.
3. Walch, S.; Dhanda, A.; Aryanpour, M.; Pitsch, H.J. Mechanism of molecular oxygen reduction at cathode of PEM fuel cells. *Journal of Physical Chemistry* **2008**, *C112*, 8464-8474.
4. Owens. F.J. Modeling boron nitride nanostructures as catalysts in fuel cells. *Molecular Simulation* **2017**, *43*, 724-727.
5. Zhang, L.; Xia, Z. Mechanism of oxygen reduction in nitroen doped graphene for fuel cells. *Journal of Physical Chemistry* **2011**, *C115*, 11170-11176.
6. Zhang, L.; Niu, J.; Dai, L. Effect of microstructure of nitrogen doped graphene on oxygen reduction activity in fuel cells. *Langmuir* **2012**, *28*, 7542 -7550.
7. Frish. M.J et.al. Gaussian 03, Revision B.04, Pitsburg PA, Gaussian Inc.

8. Miller, M.; Owens, F.J. Application of self-consistent reaction field theory to exothermic reactions in energetic materials. *Computational and Theoretical Chemistry* **2012**, *989*, 86.
9. Irikura, K.K. Systematic errors in ab initio bond dissociation energies. *Journal of Physical Chemistry* **1998**, *102*, 9031-9034.
10. Feng, L.; Liu, Y.; Zhao, J. Iron embedded boron nitride sheet for oxygen reduction reaction. *Journal of Power Sources* **2015**, *287*, 431-438
11. We,W.; Chen, W. Size dependent catalytic activity of copper nanostructures for oxygen electro-reduction. *International Journal of Smart Nano Materials* **2013**, 4, 62-71.

NEW FRONT. CHEM. (2020)
Volume 29, Number 2, pp. 69-97
ISSN 2668-9189; ISSN-L 2393-2171

Former: Ann. West Univ. Timisoara – Series Chem.
ISSN: 1224-9513

Article

TOPO-CHEMICAL REACTIVITY STUDY ON MOLECULAR MACHINES

***Nicoleta A. Dudaş*[1], *Ottorino Ori*[1,2], *and Mihai V. Putz* [1,3](♣)**
(1) Laboratory of Structural and Computational Physical-Chemistry for Nanosciences and QSAR, Biology-Chemistry Department, West University of Timisoara, Pestalozzi Street No. 16, Timisoara, RO-300115, Romania
(2) Actinium Chemical Research, Via Casilina 1626/A, 00133 Rome, Italy
(3) Laboratory of Renewable Energies-Photovoltaics, R&D National Institute for Electrochemistry and Condensed Matter, Dr. A. Paunescu Podeanu Str. No. 144, Timisoara, RO-300569, Romania

ABSTRACT

A topological-chemical reactivity studies (using electronegativity, chemical hardness, chemical power, electrophilicity indices and topological indices like Wiener indice) has been applied on calixare-based rotaxane complexes containing tris(N-phenylureido)-calix[6]arene as wheel and a 4,4'-bipyridinium dication's units as axle. The results indicate that the formation of this type of rotaxanic complex needs a preorganisational modifications undertaken by the calixarene to match with its molecular surface the shape of the guest molecule (axle of rotaxane). The obtained chemical binding scenario suggests that we are dealing with a system that remains open until the delayed maximization of the HOMO-LUMO interval, fact that allows the continuous transfer of charge between the components of the rotaxane.

Keywords: Molecular mashines, Rotaxane; Calixarene; Chemical reactivity indices, Wiener indices.

1. INTRODUCTION

Supramolecular chemistry, “the chemistry beyond the molecule” [1-3] is one of the trends of the last decades; a domain that continues to grow in many directions/fields and won two Nobel prize in the last 30 years [1-3]. Nowadays supramolecular chemistry is a highly interdisciplinary field and is composed of many expanding areas with many different

---

♣ Correspondent author: Tel: +40-256-592638, Fax: +40-256-592620; E- mails: mv_putz@yahoo.com or mihai.putz@e-uvt.ro

applications. From this point of view we can mention: mechanically interlocked molecules (MIMs), molecular machines and motors, molecular sensors (chemosensors), etc. [1-10]. In the case of these assemblies like mechanically interlocked molecules, the molecules are not chemically bonded; the molecules interact through intermolecular bonds and/or forces and come together resulting complexes with new and better properties [1-10]. A new concept introduce in the last years in supramolecular interactions is the *mechanical bond* which is the driving force for mechanically interlocked molecules (MIMs) [3,4].

Molecules that are connected as a consequence of their topology are named *Mechanically interlocked molecular architectures*; these interlocked molecules cannot be separated without the breaking of the covalent bonds that comprise the conjoined molecules. [4,10-12]. As mechanically interlocked molecular architecture are known rotaxanes and catenanes. Rotaxanes are composed of one or more axles/threads (the dumbbell components) which is surrounded by one or more rings/wheel (an macrocyclic compound) while catenanes are made of (at least) two interlocked macrocycles (rings) [4,10,13-16]. (see Figure 1). These compounds have many application in different field like chemistry, biology, medicine and in materials research, they can be used as drug delivery agents, catalysts, in molecular electronics as logic molecular switching elements, as molecular shuttles etc [4,10,15-21].

Figure 1: Schematic structures of molecular machines: *left* – rotaxanes structures, *right* – catenanes structures

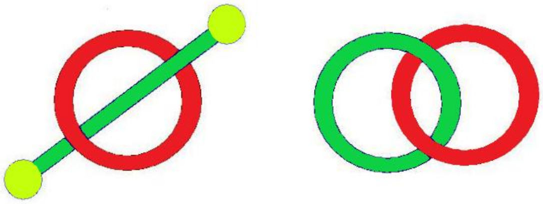

The rotaxanes axle is terminated by bulky end-groups (stoppers) that prevent that these complexes to disassembly [4,10,13-16]. If the bulky groups are too small or they do not exist, the complexes are named as pseudorotaxanes [4,10,14]. The rotaxane ring can made two molecular motions: *rotation motions* – it is rotating around the axis of the dumbbell; or *translation motions* – it is sliding along its axle from one site to another [4,10,13-16].

One of the chemical species that are used to made the dumbbell component of the rotaxanes are bipyridine unit (a dicationic viologen axle) to which are attached alkyl chains of different lengths (symmetrical or not) which may have various bulky end-groups (stoppers) [10,16,22-27]. These 4,4'-bipyridinium dications are an electron accepting units, an electron-poor π-systems that exhibit quite different physico-chemical properties (as evidenced by photophysical, photochemical and electrochemical investigations, quantum chemical calculations [10,16,25-27]) and are widely used in the construction of molecular devices [10,16,22-27] (see Figures **2** and **3**).

Calixarenes are now very popular building blocks in many diverse areas as molecular and supramolecular systems like rotaxanes, but also they are used in the synthesis of nanoparticles-based architectures and catalysis, for their biological applications, etc. [10,16,21,28-34]. All these applications of calixarenes are due to their properties like: high chemical and thermal stability, high melting points, low solubility and toxicity, their synthetic availability and the presence of reactive sides, structures that can relatively be easily modified [10,16,21,28-34].

Figure 2: *Left* - the 4,4’-bipyridinium dication unit - axle in rotaxane complex; *Right* - tris(N-phenylureido)-calix[6]arene - the calixarene wheel in rotaxane complex

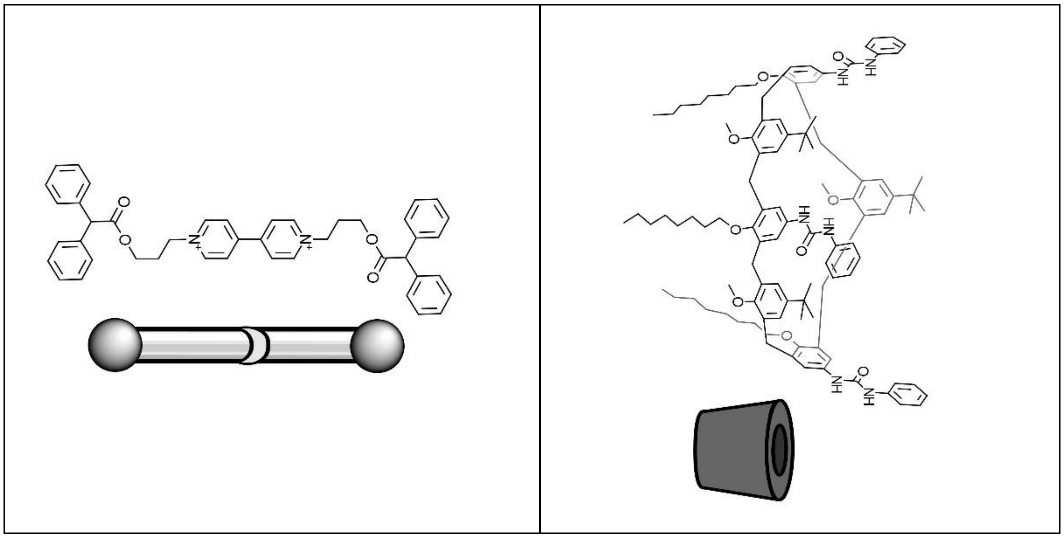

Figure 3 Calixarene-based rotaxane **1_4** which contain as wheel tris(N-phenylureido)-calix[6]arene and as axle a 4,4’-bipyridinium dication unit

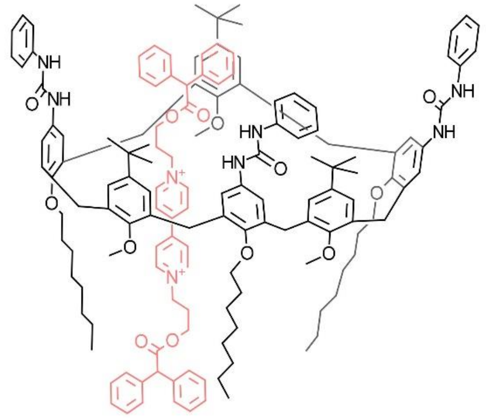

Molecular machine complexes like **1_4, 2_4 or 3_4** (see Figure **3** and **4**) are rotaxane -type systems wich contain calyx[6]arene wheel like tris(N-phenylureido)-calix[6]arene (compound **4**) and bipyridinium units as axle (compounds **1, 2, 3**), have been extensively researched in the last decades[10,16,22-27,35-44]. For the dicationic rotaxanes like **1_4, 2_4 or 3_4,** the counteranions can be tosylate, iodine, etc [10,16,22-27]. These complexes are stabilized together through solvophobic effects and several non-covalent interactions like: hydrogen bonds, CH-π and charge-transfer interactions between the π-electron poor bipyridinium unit and the π-electron rich cavity of the wheel [10,16,22,23,38]. NH-moiety from ureidic groups located on the upper rim of the wheel can make hydrogen bonds with the counteranions (e.g.: tosylate) fact that will lead to the stabilization of the complex [10,16,22,23,38]. It seems that the solvent do not affect the behavior of the central 4,4'-bipyridinium unit in the case of the complex **1_4** (see Figure **3)** [10,16,22,23,39]**..** This complex have the shortest 4,4'-bipyridinium axle wich is deeply encapsulated within the wheel–stoppers ensemble [10,16,22,23,39]. In rotaxanes (or catenanes) molecular mashines based on calix[6]arene, the wheel of rotaxane complex can present many geometries, different conformations: cone, a partial cone, [(1,2), (1,3), (1,4)]-alternate, [(1,2,3), (1,2,4), (1,3,5)]-alternate,. This geometries/conformation of the calix[6]arene depend on the type and number of the substituents situated on upper or lower rim [22-27,31,35-46] and have been very intense investigated in the last years (the synthesis, co-conformational switching, atropoisomerism, their properties (e.g. redox properties), etc.) [22-27,31,40-46].

Figure 4: Structures of the three 4,4'-bipyridinium dication unit **-** axle in rotaxane complex (**1, 2, 3**) and the tris(N-phenylureido)-calix[6]arene (**4**) **-** the calixarene wheel in rotaxane complex

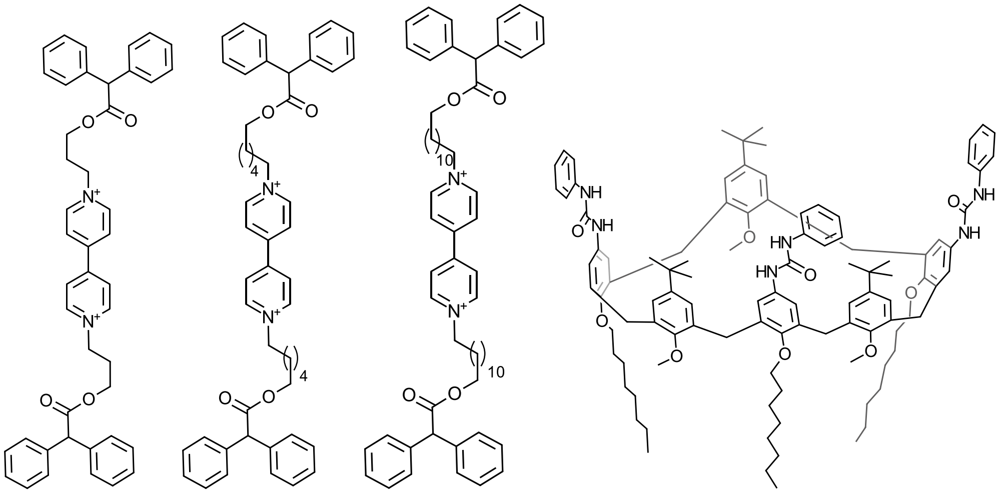

1 **2** **3** **4**

So far, in the literature can be found studies that reveal the mechanism of chemical-biological interaction between the biological receptor and the chemical ligand using the chemical reactivity indicators [10,47,48] and topological relation between chemical structure and biological activity [49]. Referring to calixarenes, rotaxane and molecular machines it seems that are missing topological-chemical reactivity studies (such as those who are using electronegativity, chemical hardness, chemical power, electrophilicity indices and topological indices like Wiener indice).

2. METHOD

2.1. Theoretical Model

The molecular orbitals HOMO and LUMO, provides basic chemical reactivity indices. The molecular structure include the key pathway to chemical reactivity through their HOMO and LUMO. This chemical reactivity indices combine with their associated chemical principles can be interpreted in QSAR models and not only [10,47,48,50]. This basic chemical reactivity indices are electronegativity (χ), chemical hardness (η), chemical power index (π), electrophilicity (ω) which are defined:

- electronegativity (χ) is negative of the chemical potential [10,47,51-54], through the derivation of the total energy with respect of the total number of electrons, reducing in the finite/central difference approximation to the celebrated Mulliken formula [10,47,55]:

$$\chi \equiv -\mu \equiv -\left(\frac{\partial E_N}{\partial N}\right)_{V(\mathrm{r})} \cong -\frac{E_{LUMO} + E_{HOMO}}{2} \tag{1}$$

- chemical hardness (η) is the negative variation of electronegativity with respect of the total electrons in the system [10,47,56-59], also approximates in the finite difference with HOMO–LUMO information simply as [10,47,60]:

$$\eta = -\chi \equiv -\frac{1}{2}\left(\frac{\partial \chi}{\partial N}\right)_{V(\mathrm{r})} \equiv \left(\frac{\partial^2 E_N}{\partial N^2}\right)_{V(\mathrm{r})} \cong \frac{E_{LUMO} - E_{HOMO}}{2} \tag{2}$$

- chemical power index (π) is the half ratio of electronegativity-to-chemical hardness that models the electronic charges exchanged through the adducts in minimizing the resulting bonded complex electronegativity [10,47,50]:

$$\pi = \frac{\lambda}{2\eta} = \frac{1}{2}\frac{\chi_A}{\eta_B} = \frac{1}{2}\tan(\theta_A) \cong -\Delta N_A \tag{3}$$

- electrophilicity (ω) is the coupling of chemical power index with electronegativity to provide the energetic information of activation towards charge tunneling of the potential barrier between adducts [10,47]:

$$\omega = \chi \times \pi = \frac{\chi^2}{2\eta} \tag{4}$$

Chemical principles of this chemical reactivity indices are [10,47,48]:

- Minimum electronegativity principle eqs. (5)
- Maximum hardness principle eqs. (6)
- Minimum chemical power index principle eqs. (7)
- Minimum electrophilicity principle (double minimum character) eqs. (8)

$$\delta\chi \le 0 \tag{5}$$

$$\delta\eta \ge 0 \tag{6}$$

$$\delta\pi \le 0 \tag{7}$$

$$\delta\omega \leq 0 \tag{8}$$

The hierarchy for chemical binding scenario [10,61] is leaving with the conducted hierarchy eqs. (9) [10,47,48,61,62]:

$$\chi \to \eta \to \pi \to \omega \tag{9}$$

Namely a chemical reaction/interaction is triggered by electronegativity (its difference) and its minimizing principle, followed by chemical hardness maximization of the interacting frontier orbitals implying maximum energy in charge exchange (parallel spins) followed by minimum activation by adducts' potential barrier tunneling (spin pairing) [10,47,48,61,62]. However, when is about a chemical interaction through non-covalent bonding and/or mechanical bonding, such chemical hierarchy is may lead with various hierarchical configurations [10,47,48].

Topological indices like *Wiener index W* have been successfully applied to emphasize *the stability of the chemical structure* [49,63-66]. The *Wiener index W* of the whole chemical graph G is the sum of the *Wiener-weights* w_v [49,63-66]:

$$W = \sum_{v=1}^{N} w_v \tag{10}$$

In the chemical graph G with N nodes and B bonds, the *chemical distance* d_{vu} is merely the number of bonds connecting, along the shortest path, any pairs of atoms in the system, namely the two nodes *v* and *u*, with $d_{vv}=0$ by definition [49,63-66]. With the name *Wiener-weight* w_v of the node *v* we call the the half-summation of the minimum distances d_{uv} between all pairs of G(N) vertices, meaning the invariant [49,63-66]:

$$w_v = \frac{1}{2}\sum_{u=1}^{N} d_{uv},\, d_{vv} = 0, u, v = 1,2,\ldots, N \tag{11}$$

The *Wiener-weight* w_v it is inversely proportional to the *reactivity* of the node and to the *compactness* of the graph. *The Wiener index W* of the whole graph is just the sum of the Wiener-weights eqs. (10) [49,63-66]. Also the *Wiener-weight* w_v allows the direct topological measure of the topological roundness of the graph: *the topological efficiency index* ρ and the *extreme topological efficiency index* ρ^E [49,63-66]:

$$\rho = {WN}\big/{\underline{w}} \tag{12}$$

$$\rho^E = {\overline{w}}\big/{\underline{w}} \tag{13}$$

in which $\underline{w}$ = min{ w_v } and $\overline{w}$ = max{ w_v }.

It is noticeable that the most compactly-embedde vertices of G (the so-called *minimal vertices or minimal nodes*) have Wiener-weight w_v equal to $\underline{W}$ and also that *the smallest is the topological efficiency index, the highest is the stability of the chemical structure under examination* eqs. (14), eqs. (15) [49,63-66].

$$\rho \geq 1 \tag{14}$$

$$\rho^E \geq 1 \tag{15}$$

Table 1. Total energy and the parameters of chemical reactivity calculated for rotaxanes **1_4, 2_4, 3_4** under study, which are in the precomplex stage as well as complexes; Δ – is the differences between complex and precomplex state.

PRECOMPLEX	**$\mathrm{HOMO}_{precomplex}$**	**$\mathrm{LUMO}_{precomplex}$**	**$\chi_{precomplex}$ (eV)**	**$\eta_{precomplex}$ (eV)**	**$\pi_{precomplex}$**	**$\omega_{precomplex}$ (eV)**	**$\mathrm{Etotal}_{precomplex}$ (kcal/mol)**
1:4	110.8641	117.7821	-114.3231	3.459	-16.52545533	1889.241283	3702346.613
2:4	82.58545	84.71627	-83.65086	1.06541	-39.25759097	3283.931247	3621720.058
3:4	-144.966	-143.0296	143.9978	0.9682	74.36366453	10708.20409	3477598.596
COMPLEX	**$\mathrm{HOMO}_{complex}$**	**$\mathrm{LUMO}_{complex}$**	**$\chi_{complex}$ (eV)**	**$\eta_{complex}$ (eV)**	**$\pi_{complex}$**	**$\omega_{complex}$ (eV)**	**$\mathrm{Etotal}_{complex}$ (kcal/mol)**
1_4	-5.43268	-5.06872	5.2507	0.181979	14.42666	75.75009	3837167.691
2_4	32.81105	33.90942	-33.360235	0.549185	-30.37249288	1013.2335	3870660.029
3_4	-88.8077	-87.3996	88.10365	0.704085	62.56606	5512.298	4045342.867
Δ=Complex -Precomplex	**$\Delta\mathrm{HOMO}_{complex-precomplex}$**	**$\Delta\mathrm{LUMO}_{complex-precomplex}$**	**$\Delta\chi_{complex-precomplex}$ (eV)**	**$\Delta\eta_{complex-precomplex}$ (eV)**	**$\Delta\pi_{complex-precomplex}$**	**$\Delta\omega_{complex-precomplex}$ (eV)**	**$\Delta\mathrm{Etotal}_{complex-precomplex}$ (kcal/mol)**
Case 1_4	-116.296779	-122.850821	119.5738	-3.277021	30.95211995	-1813.491195	134821.0774
Case 2_4	-49.7744	-50.80685	50.290625	-0.516225	8.885098099	-2270.697747	248939.9723
Case 3_4	56.15827	55.63004	-55.894155	-0.264115	-11.79760717	-5195.906385	567744.2707

2.2. Computational Model

For our study we choose the molecular mashine complexes **1_4, 2_4, 3_4** formed from the 4,4'-bipyridinium dication unit **1, 2 and 3** and the wheel of rotaxane made of calyx[6]arene with three N-phenylureido groups on the upper rim of the wheel **(4)** (see Figure 3 and 4) [22,23,39]**.**

We have calculated the chemical reactivity parameters (electronegativity (χ), chemical hardness (η), chemical power index (π), electrophilicity (ω)) for the two stages of the rotaxane molecular machine: precomplexes **(1:4, 2:4, 3:4)** and rotaxane molecular complexes **(1_4, 2_4, 3_4)**. The values of HOMO, LUMO orbitals energies are calculated using the semiempirical method (AM1) (Polak-Ribiere conjugate gradient algorithm and single point geometry optimization) as provided by Hyperchem 7.01 [67], while the values of chemical reactivity parameters were calculated using those for HOMO and LUMO and Eqs. (1), (2), (3), and (4) (see Table 1). For all stages (precomplex and complex) also was calculated the total energy using the same semiempirical method (AM1) and also was calculated the difference between the complex and precomplex stage. All the results are summarized in Table 1.

The molecular structures of calix[6]arenes complexes with three kinds of guest, molecular complexes **1_4, 2_4, 3_4** in the partial cone conformation have been herewith studied by ab-initio and topological methods (see Table 2). Energy calculations have been performed to gain more insight on the stabilizing effects coming by the host-guest interactions.

Table 2. *Wiener index W, the topological efficiency index* ρ and the *extreme topological efficiency index* ρ^E for the complexes in work

Rotaxane complex	**W**	**ρ**	**ρ^e**	**W_{exp}**
1_4	13719	1.322313	1.703614	*35.92726*
2_4	20786	1.32092	1.701068	*39.41446*
3_4	40968	1.324111	1.716484	*46.39794*

3. RESULTS AND DISCUSSIONS

We performed the correlation between the total energy, the chemical reactivity indices and the Wiener indices for the rotaxane molecular complexes (**1_4, 2_4, 3_4),** and for the Δ-stage (the difference between the complex and precomplex stage), the results being included in Table 3.

Table 3: Correlation between the energy, the chemical reactivity indices and the Wiener indices for the rotaxane molecular complexes (**1_4, 2_4, 3_4),** and also for the Δ-stage (the difference between the complex and precomplex stage)

The linear regression equation and the graph of the obtained equation, R and R^2 values	**The linear regression equation and the graph of the obtained equation, R and R^2 values**
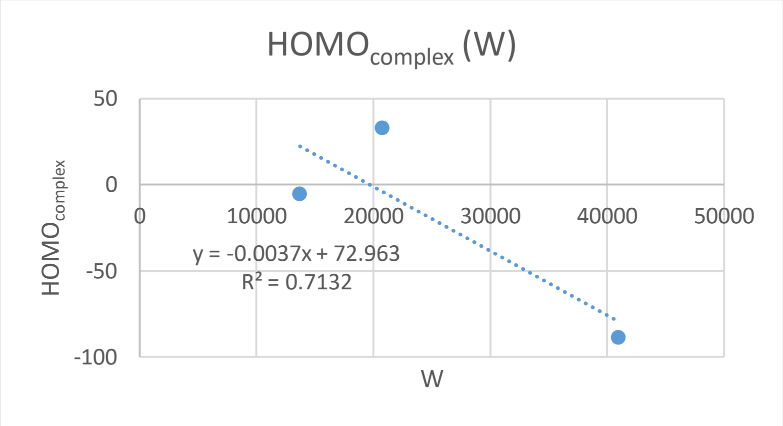 $\mathbf{HOMO_{complex}(W)} = -0.003714\ \mathbf{W} + 72.96345$ R = 0.84453578	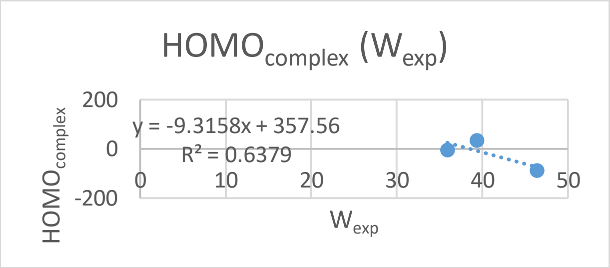 $\mathbf{HOMO_{complex}(W_{exp})} = -9.315836\ \mathbf{W_{exp}} + 357.559148$ R = 0.79868301
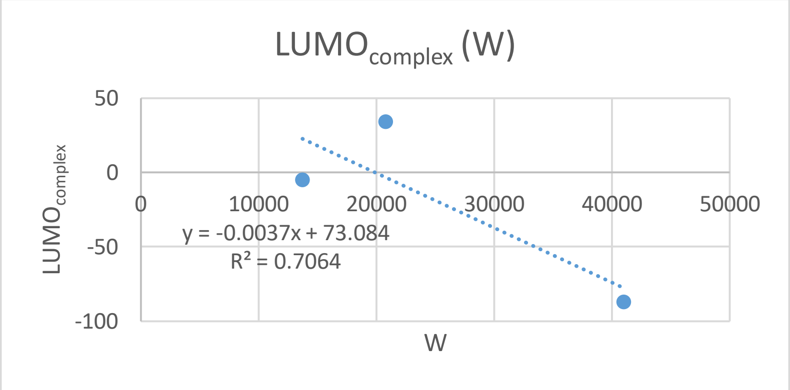 $\mathbf{LUMO_{complex}(W)} = -0.00368\ \mathbf{W} + 73.083705$ R = 0.8327144	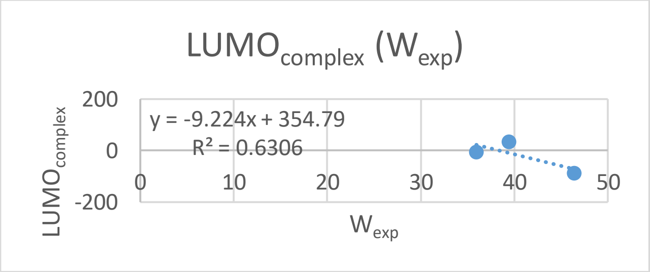 $\mathbf{LUMO_{complex}\ (W_{exp})} = -\ 9.22403465\ \mathbf{W_{exp}} + 354.790675$ R = 0.79409727

<table>
<tr>
<th>The linear regression equation and the graph of the obtained equation, R and R² values</th>
<th>The linear regression equation and the graph of the obtained equation, R and R² values</th>
</tr>
<tr>
<td>
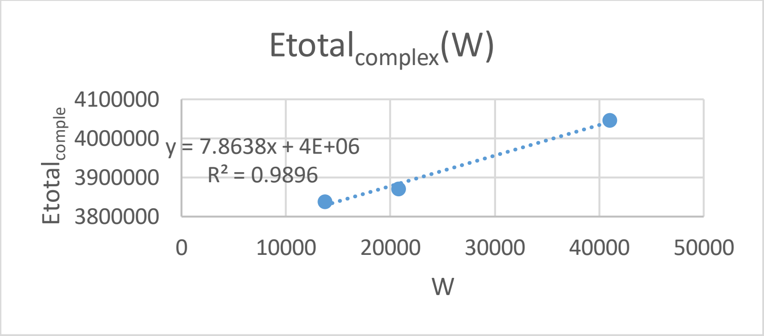

$\mathbf{Etotal_{complex}(W)} = 7.8638\ \mathbf{W} + 3719888.59$ R = 0.99478401
</td>
<td>
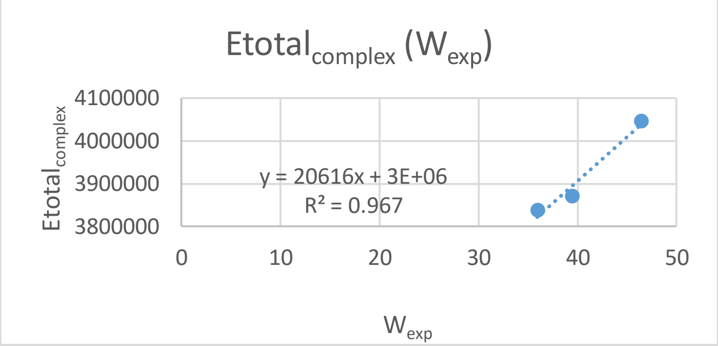

$\mathbf{Etotal_{complex}(W_{exp})} = 20616.3738\ \mathbf{W_{exp}} + 3081113.38$ R = 0.98334296
</td>
</tr>
<tr>
<td>
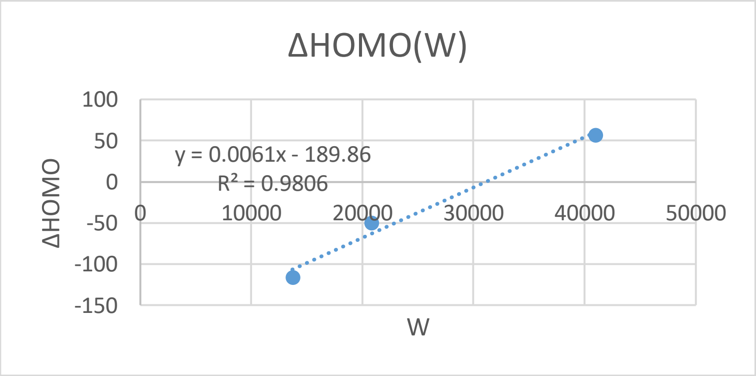

$\mathbf{\Delta HOMO(W)} = 0.00609\ \mathbf{W} - 189.862798$ R = 0.99023547
</td>
<td>
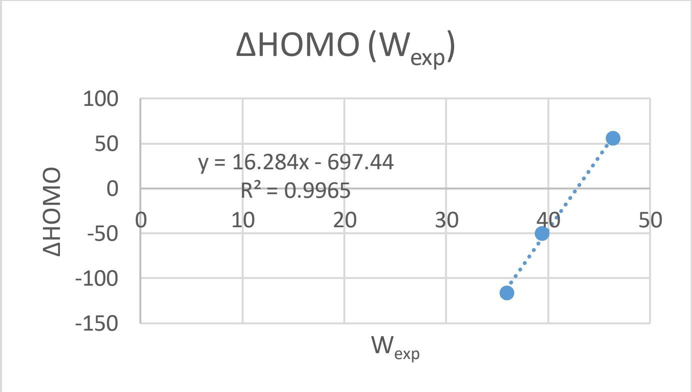

$\mathbf{\Delta HOMO\ (W_{exp})} = 16.284015\ \mathbf{W_{exp}} - 697.44118$ R = 0.99824428
</td>
</tr>
</table>

The linear regression equation and the graph of the obtained equation, R and R^2 values	**The linear regression equation and the graph of the obtained equation, R and R^2 values**
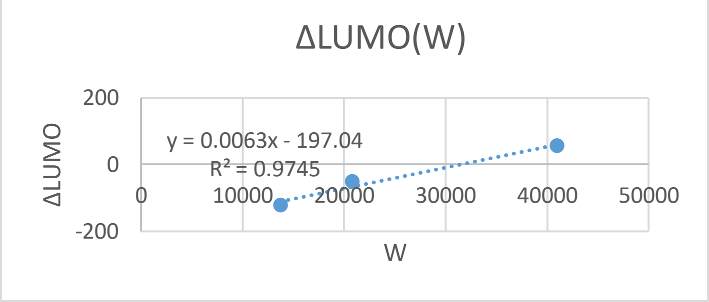 **ΔLUMO(W) = 0.**006268 **W-**197.042346 R = 0.98718854	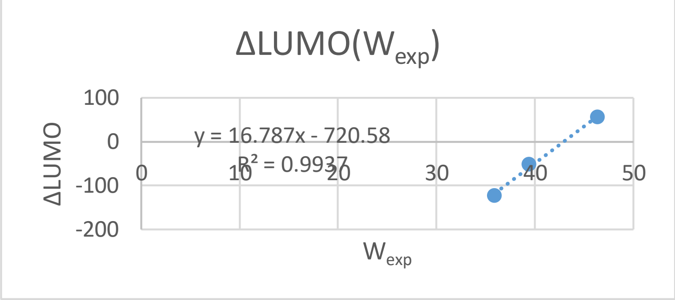 **ΔLUMO(W_{exp})** = 16.78746 **W_{exp} -** 720.57596 R = 0.99682972
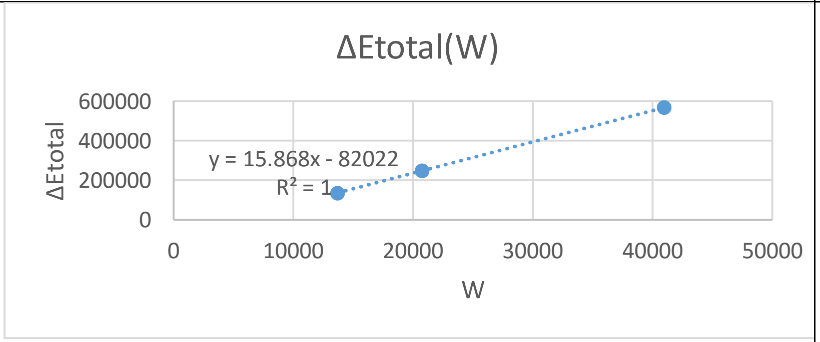 **ΔEtotal (W)** = 15.86755 **W** -82022.1259 R = 0.99998959	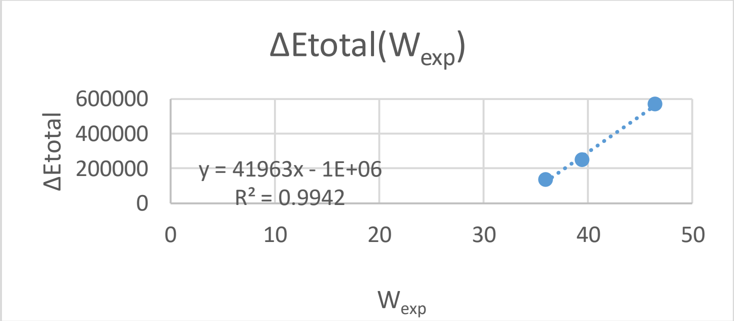 **ΔEtotal (W_{exp})** = 41962.504 **W_{exp}** -1385665.29 R = 0.99711105

The linear regression equation and the graph of the obtained equation, R and R^2 values	**The linear regression equation and the graph of the obtained equation, R and R^2 values**
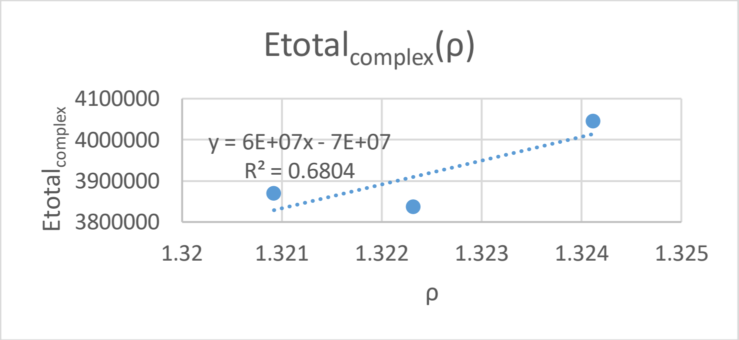 $\mathbf{Etotal_{complex}(\rho)} = 57636021.9\ \boldsymbol{\rho}\ - 72302930.135$ R = 0.82485348	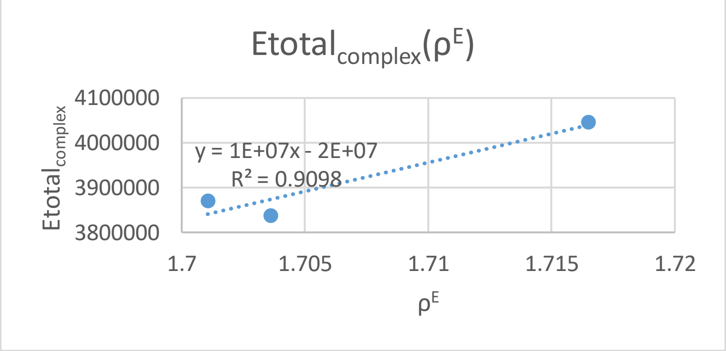 $\mathbf{Etotal_{complex}\ (\rho^E)} = 12902072.77\ \boldsymbol{\rho^E}\ - 18106826.89$ R = 0.95382083
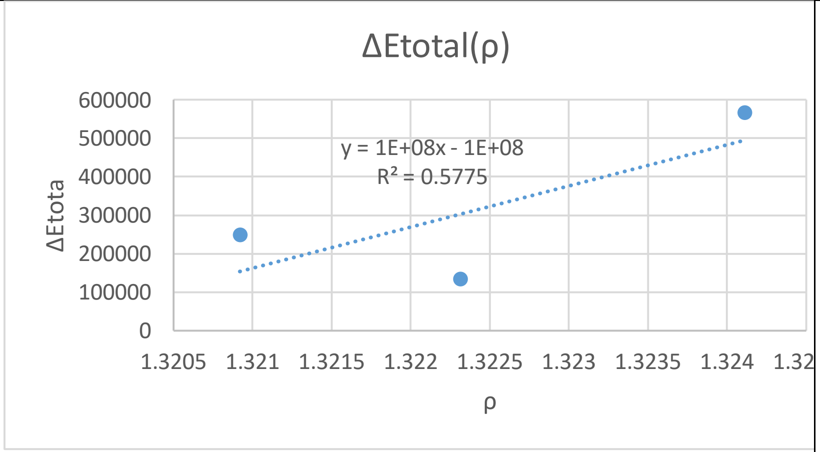 $\mathbf{\Delta Etotal(\rho)} = 106585627.65\ \boldsymbol{\rho}\ - 140636803.35$ R = 0.75992522	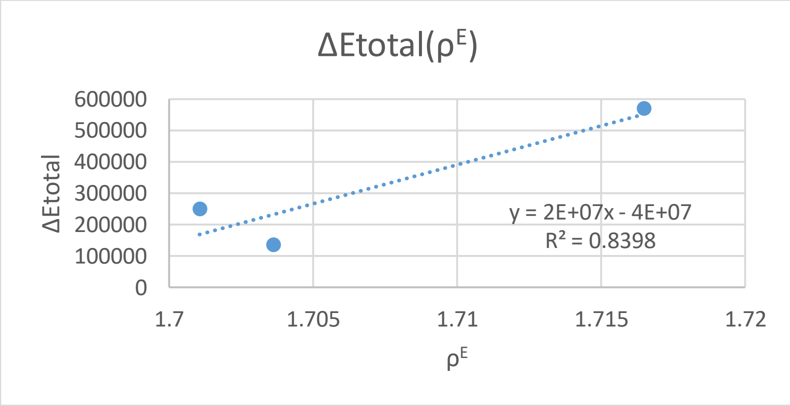 $\mathbf{\Delta Etotal(\rho^E)} = 24881879.8\ \boldsymbol{\rho^E}\ - 42157573.89$ R = 0.91638907

The linear regression equation and the graph of the obtained equation, R and R^2 values	**The linear regression equation and the graph of the obtained equation, R and R^2 values**
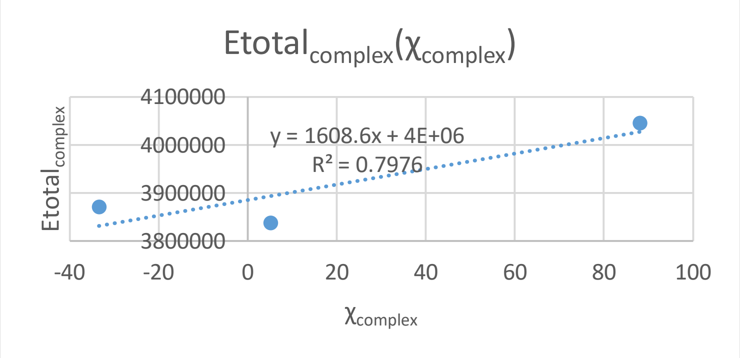 **Etotal**$_{\mathbf{complex}}$ **(χ**$_{\mathbf{complex}}$**)** = 1608.57629 **χ**$_{\mathbf{complex}}$ + 3885555.16 R = 0.89305771	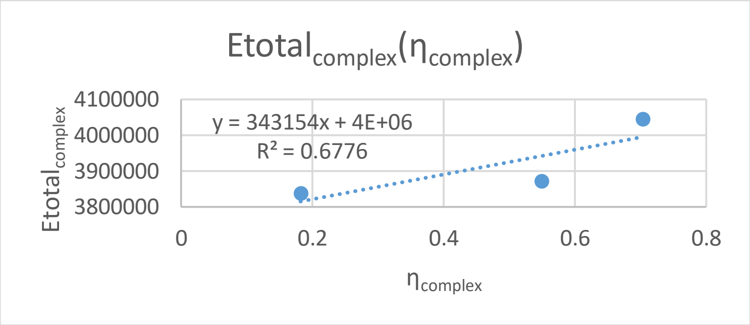 **Etotal**$_{\mathbf{complex}}$ **(η**$_{\mathbf{complex}}$**)** = 343153.77 **η**$_{\mathbf{complex}}$ + 3753553.15 R = 0.82317418
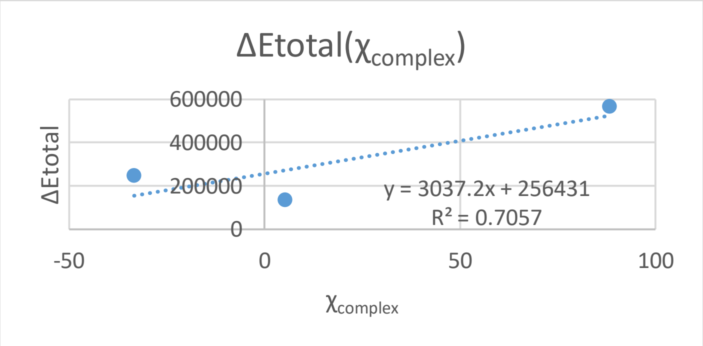 **ΔEtotal (χ**$_{\mathbf{complex}}$**)** = 3037.183289 **χ**$_{\mathbf{complex}}$ + 256430.73 R = 0.84003670	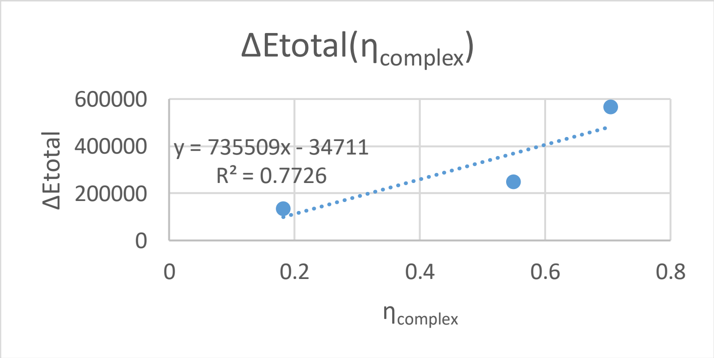 **ΔEtotal (η**$_{\mathbf{complex}}$**)** = 735508.68 **η**$_{\mathbf{complex}}$ - 34710.9273 R = 0.87898236

The linear regression equation and the graph of the obtained equation, R and R^2 values	**The linear regression equation and the graph of the obtained equation, R and R^2 values**
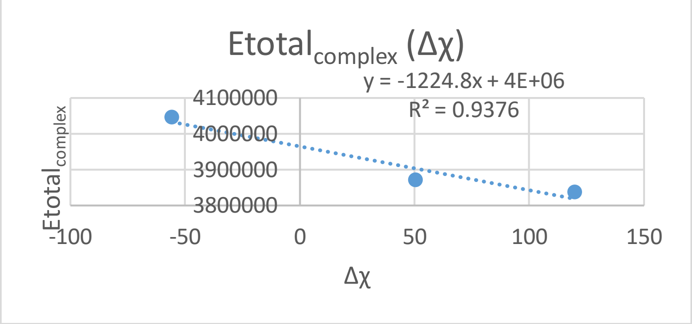 $\mathbf{Etotal_{complex}\ (\Delta\chi)} = -\ 1224.751\ \mathbf{\Delta\chi} + 3964251.93$ R = 0.96831697	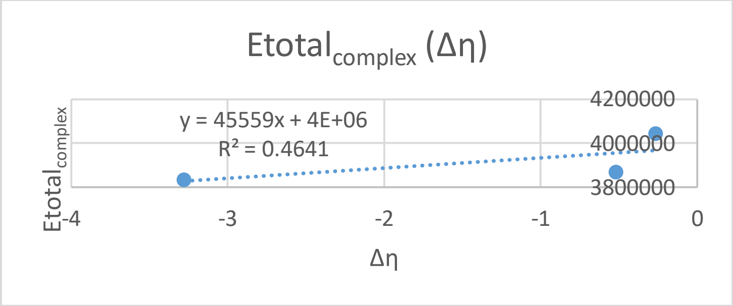 $\mathbf{Etotal_{complex}\ (\Delta\eta)} = 45559.262\ \mathbf{\Delta\eta} + 3979340.32$ R = 0.68124434
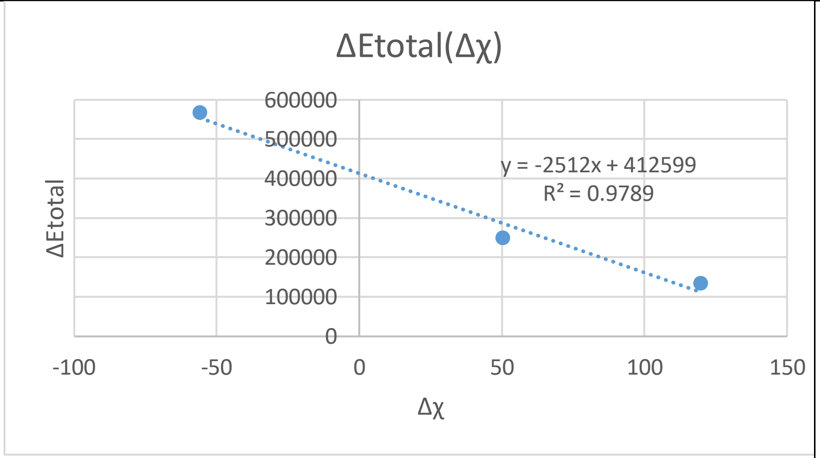 $\mathbf{\Delta Etotal\ (\Delta\chi)} = \mathbf{-}\ 2511.99\ \mathbf{\Delta\chi} + 412599.17$ R = 0.98941168	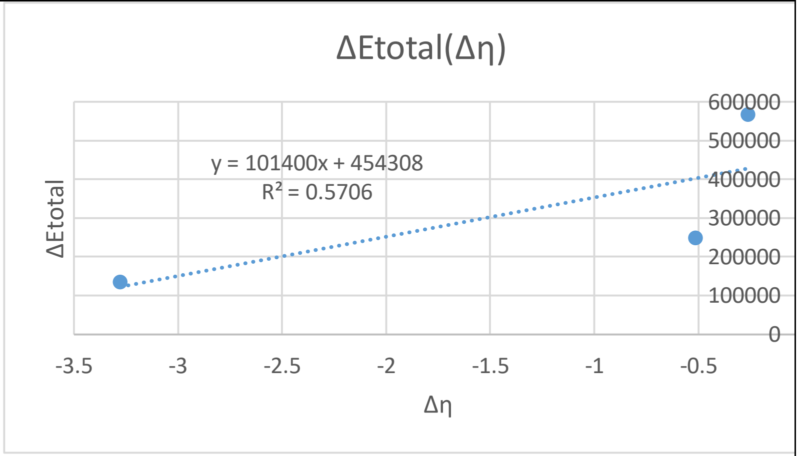 $\mathbf{\Delta Etotal \Delta\eta)} = 101400.33\mathbf{\Delta\eta} + 454307.68$ R = 0.75536176

The linear regression equation and the graph of the obtained equation, R and R^2 values	**The linear regression equation and the graph of the obtained equation, R and R^2 values**
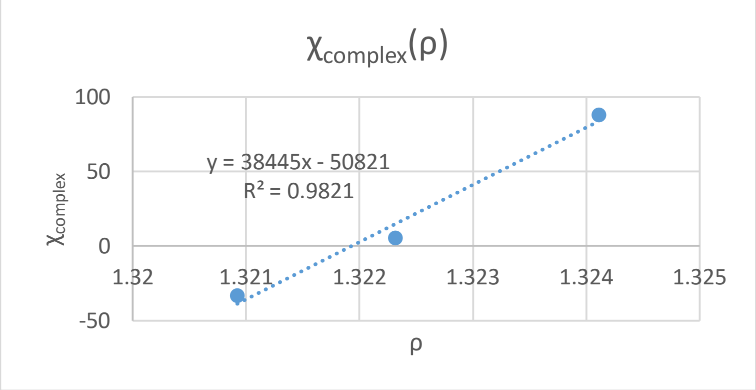 $\chi_{complex}(\rho) = 38444.59\ \rho - 50820.985\ 2 \quad R = 0.99101500$	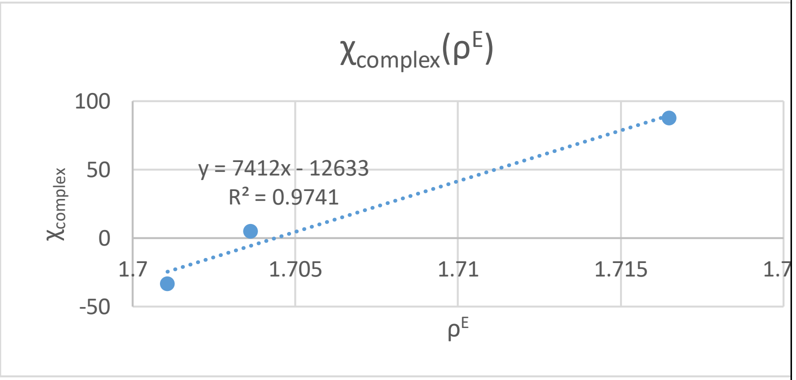 $\chi_{complex}(\rho^E) = 7411.976\ \rho^E - 12632.6546 \quad R = 0.98696893$
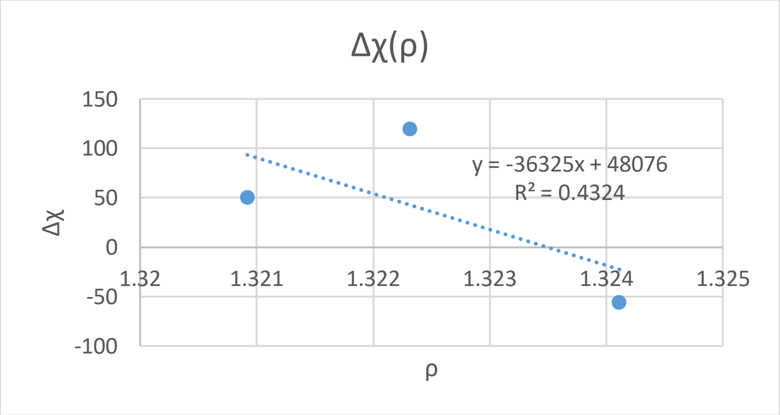 $\Delta\chi(\rho) = -36325.22\ \rho + 48076.217 \quad R = 0.65753883$	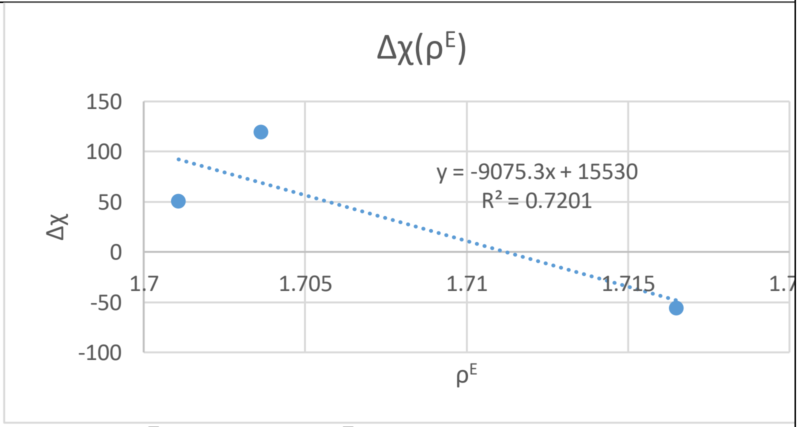 $\Delta\chi(\rho^E) = -9075.282\ \rho^E + 15529.99 \quad R = 0.84858966$

The linear regression equation and the graph of the obtained equation, R and R^2 values	**The linear regression equation and the graph of the obtained equation, R and R^2 values**
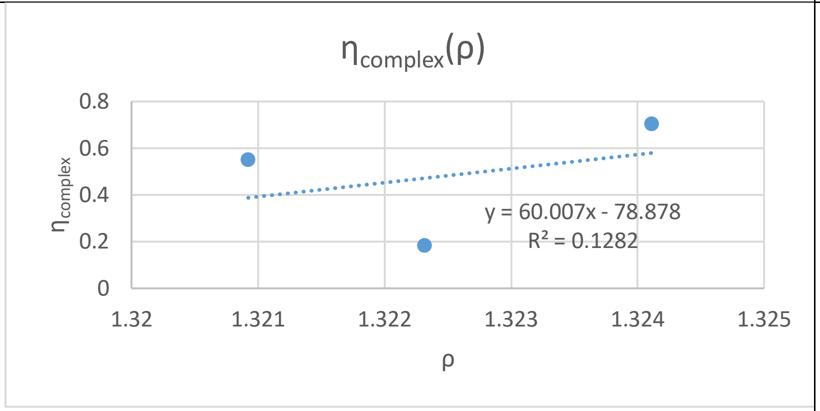 $\boldsymbol{\eta_{complex}(\rho)} = 60.00727\ \boldsymbol{\rho} - 78.87809$ R = 0.35800058	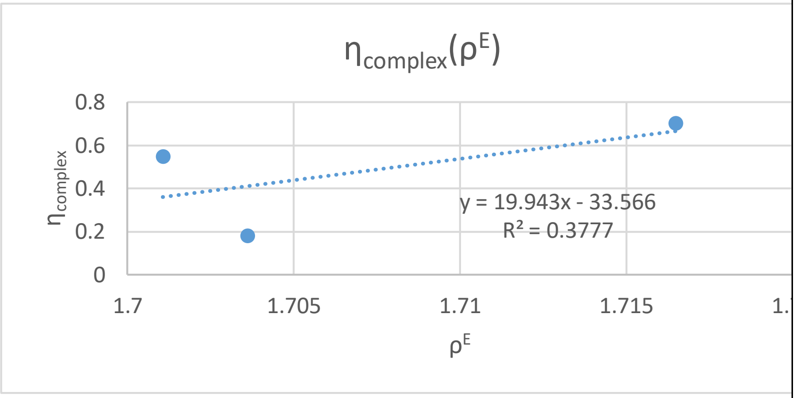 $\boldsymbol{\eta_{complex}(\rho^E)} = 19.94323\ \boldsymbol{\rho^E} - 33.565784$ R = 0.61461044
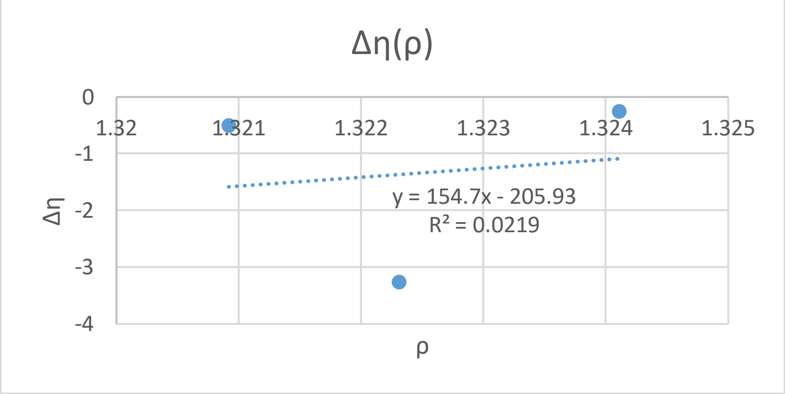 $\boldsymbol{\Delta\eta(\rho)} = 154.698159\ \boldsymbol{\rho} - 205.93275$ R = 0.14806136	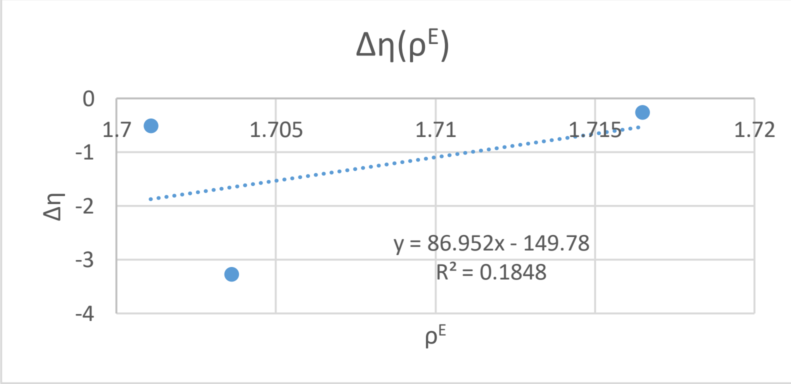 $\boldsymbol{\Delta\eta(\rho^E)} = 86.9519\ \boldsymbol{\rho^E} - 149.784165$ R = 0.42989285

The linear regression equation and the graph of the obtained equation, R and R^2 values	**The linear regression equation and the graph of the obtained equation, R and R^2 values**
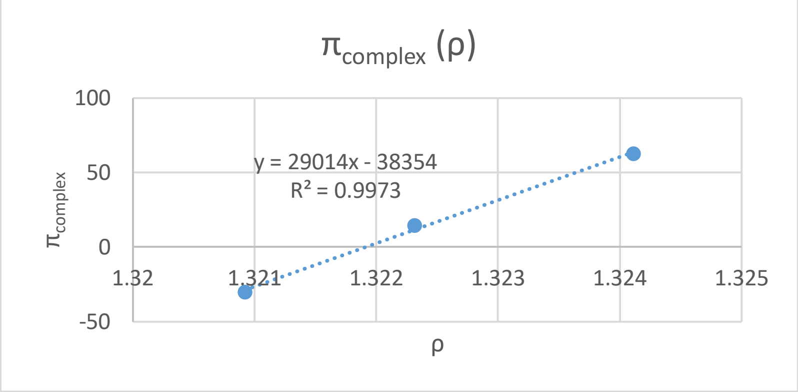 $\boldsymbol{\pi_{complex}(\rho)} = 29013.7989\ \boldsymbol{\rho} - 38353.706$ R = 0.99862880	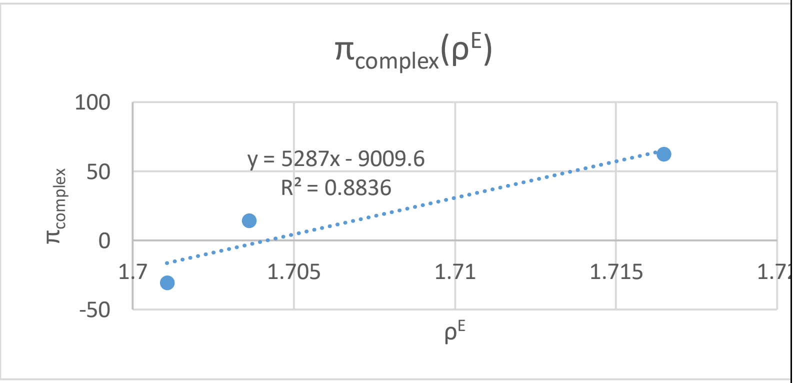 $\boldsymbol{\pi_{complex}(\rho^E)} = 5286.983\ \boldsymbol{\rho^E} - 9009.6319$ R = 0.94000878
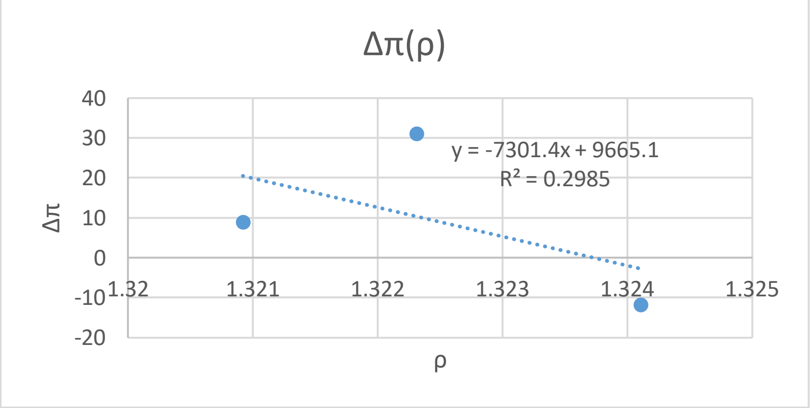 $\boldsymbol{\Delta\pi(\rho)} = -7301.444\ \boldsymbol{\rho} + 9665.1284$ R = 0.54637196	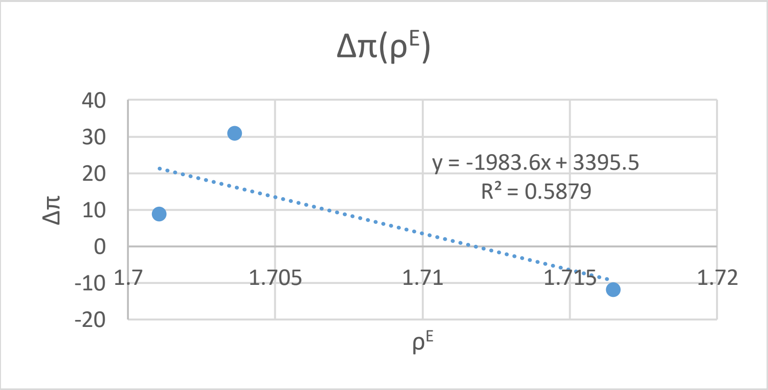 $\boldsymbol{\Delta\pi(\rho^E)} = -\ 1983.629\ \boldsymbol{\rho^E} + 3395.51075$ R = 0.76676906

<table>
<tr><th>The linear regression equation and the graph of the obtained equation, R and R^2 values</th><th>The linear regression equation and the graph of the obtained equation, R and R^2 values</th></tr>
<tr><td>
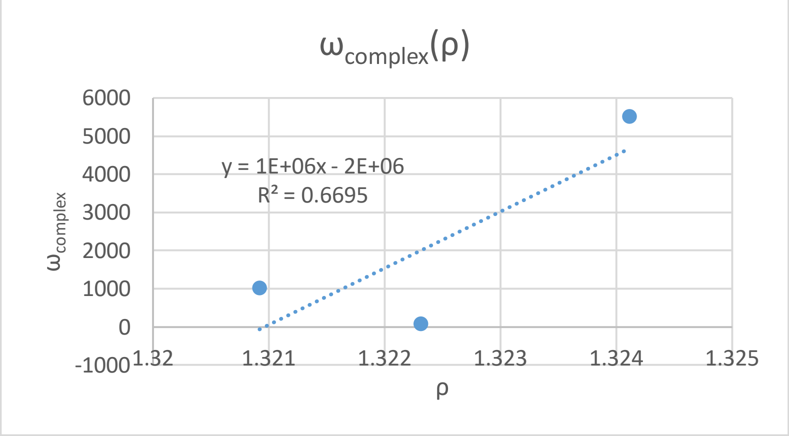

$\omega_{complex}(\rho)$ = 1486425.2 ρ - 1963519.926 R = 0.81822780
</td><td>
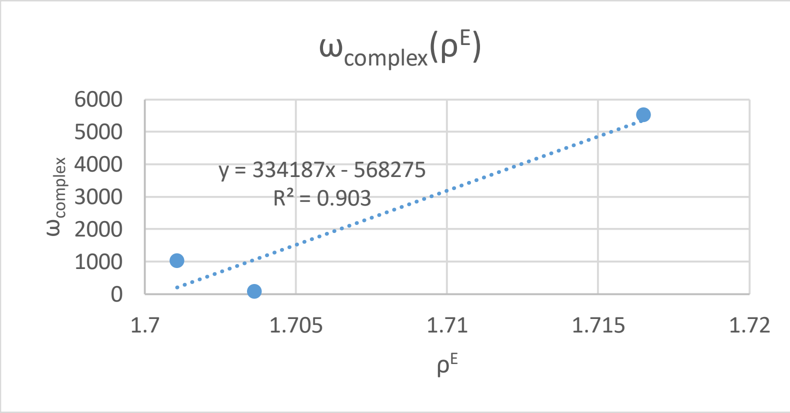

$\omega_{complex}(\rho^E)$ = 334186.87 ρ^E - 568275.01 R = 0.950265709
</td></tr>
<tr><td>
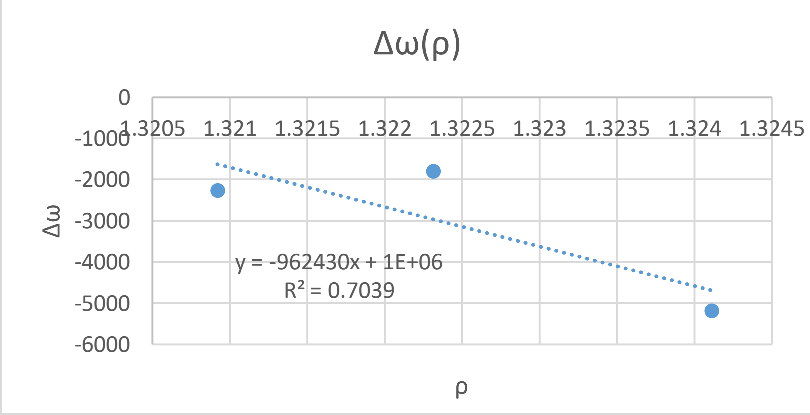

$\Delta\omega(\rho)$ = - 962430.08 ρ + 1269670.5 R = 0.83899019
</td><td>
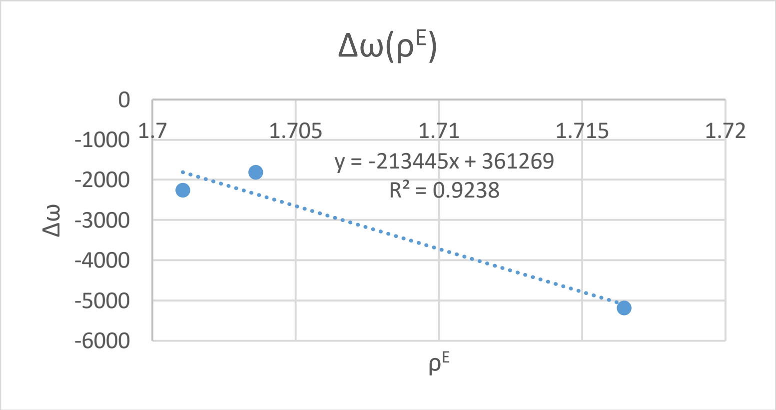

$\Delta\omega(\rho^E)$ = -213444.768 ρ^E + 361268.637 R = 0.96116448
</td></tr>
</table>

Analyzing the results **from the chemical reactivity indices point of view** (see Table 3) it can be observed the following:

- HOMO$_{complex}$, LUMO$_{complex}$ have approximately the **same** degree of correlation R^2, with W respectively W$_{exp}$. Also the same degree of correlation have ΔHOMO, ΔLUMO with W respectively W$_{exp}$.
- For ΔHOMO the degree of correlation R^2 with W respectively, W$_{exp}$ **increases** comparavetely with HOMO$_{complex}$. The same situation is also for ΔLUMO comparavetely with LUMO$_{complex}$:
  - ❖ R^2 : HOMO$_{complex}$≈LUMO$_{complex}$ for W respectively W$_{exp}$
  - ❖ R^2 : ΔHOMO≈ ΔLUMO W for respectively W$_{exp}$
  - ❖ R^2 : ΔHOMO>HOMO$_{complex}$ for W respectively W$_{exp}$
  - ❖ R^2 : ΔLUMO> LUMO$_{complex}$ for W respectively W$_{exp}$.
- Etotal$_{complex}$ and ΔEtotal have approximately the **same** degree of correlation R^2 with W respectively W$_{exp}$,
- In case of corelation between Etotal$_{complex}$ respectively ΔEtotal with **ρ** and **ρ^E** , degree of correlation R^2 it is **better** in bouth cases for **ρ^E**; when we compare Etotal$_{complex}$ with ΔEtotal degree of correlation R^2 it is **better** for Etotal$_{complex}$.
  - ❖ R^2 : **ρ^E > ρ** for. Etotal$_{complex}$ respectively ΔEtotal
  - ❖ R^2 : Etotal$_{complex}$ > ΔEtotal for **ρ^E si ρ**
- In case of corelation between Etotal$_{complex}$ respectively ΔEtotal with χ, Δχ, η, respectively Δη comparing the degree of correlation R^2 , it is observed that in the case of ΔEtotal correlation with Δχ the degree of correlation is extremely **good,** the entire comparation can be summarized as following:

R^2 **for Etotal$_{complex}$**	$\chi_{complex} > \eta$	$\Delta\chi > \Delta\eta$	$\Delta\chi > \chi_{complex}$	$\Delta\eta > \eta_{complex}$
R^2 **for ΔEtotal**	$\eta > \chi_{complex}$	$\Delta\chi > \Delta\eta$	$\Delta\chi > \chi_{complex}$	$\Delta\eta > \eta_{complex}$
R^2 **for λ**	Etotal$_{complex}$ > ΔEtotal			
R^2 **for η**	ΔEtotal > Etotal$_{complex}$			
R^2 **for Δλ**	ΔEtotal > Etotal$_{complex}$			
R^2 **for Δη**	ΔEtotal > Etotal$_{complex}$			

Observing the degree of correlation **R^2** between **ρ** and **ρ^E** with the chemical reactivity indices, it reveals that in the case of the **stable** complex of molecular mashines type / rotaxane type as against of hierarchy *for chemical binding scenario* [10,47,48,61,62]

$$\chi\rightarrow\eta\rightarrow\pi\rightarrow\omega \tag{9}$$

the hierarchy is as follows:

*The case of the **stable** complex of molecular mashines type / rotaxane type*	**π→**	**χ →**	**ω →**	**η**
R^2 for **ρ**	0.99725948	0.98211073	0.66949673	0.12816441
	χ →	**ω →**	**π→**	**η**
R^2 for **ρ^E**	0.97410766	0.90300490	0.88361651	0.377745992

and for difference (Δ) of chemical reactivity indices, in the case of the **kinetic** complex of molecular mashines type / rotaxane type the hierarchy is as follows:

The case of the **kinetic** *complex of molecular mashines type / rotaxane type*	**Δω →**	**Δχ →**	**Δπ →**	**Δη**
R^2 for $\boldsymbol{\rho}$	0.70390454	0.43235731	0.29852232	0.02192217
R^2 for $\boldsymbol{\rho}^{\mathbf{E}}$	0.92383715	0.72010442	0.58793478	0.18480786

From the topological point of view:

These molecular structures of calix[6]arenes complexes **1_4, 2_4, 3_4** with three kinds of guest molecules, 4,4’-bipyridinium dications, compounds **1, 2, 3,** and the host tris(N-phenylureido)-calix[6]arene **-** the calixarene wheel in rotaxane complex compound **4** have been herewith studied by ab-initio and topological methods. Energy calculations have been performed to gain more insight on the stabilizing effects coming by the host-guest interactions.

The simulation of the total potential energy indicates that the contribution which comes from the electrostatic polarization induced by the electric field of the guest gives a net stabilizing contribution whose values are listed in Table 4 below. Remarkably, the structural features of the present calix[6]arene derivatives confirm the validity of the "preorganization" principle early reported in literature that relies on appropriate variations of the molecular geometry of the ligands. The principle attributes an important role to the carbon/oxygen-chains of the host molecule which undertake specific the rearrangements to optimize the steric interface near the guest molecules. The preorganization mechanisms may vary, and may take place on different timescale, transforming the partial cone of the calix[6]arene to prepare it to form the new complexes **1_4, 2_4, 3_4.** Previous studies have determined that in these complexes the polar cage around the guest specie (molecules or even single cations) has normally the role of defining the position of the guest itself in respect to the barycentre of the interacting regions in the host, regions that quite often coincide with the volumes occupied by the nearest neighbor oxygens. In the present case in fact one may observe that the most significant structural deformations which preorganize the molecular structure of the polar cage to allow the formation of the complexes still consist in a geometrical distortion of the chains containing the oxygen atoms, see **Figure 5**. In these chains, topology attributes the highest the w_i=1006 (highest topo-reactivity) to the three terminal carbon atoms C37,C75,C114. Each chain starts form with an oxygen atom that functions like a sort of atomic hinge between the calixarene cone and the chain (**Figure 5**). *Vice versa, the carbon pairs C14/C16, C52/C54*, represent the most stable atoms in the core region of the topological structure of the ligand. The graphical representation of the complex **1_4** evidences large deformations in the structure of its ligand **4** that shows an almost flattened shape having lost the characteristics conic-shape. This flat structure, evidenced in **Figure 5**, is the proof of the massive preorganisational modifications undertaken by the calixarene to match with its molecular surface the shape of the guest molecule.

Figure 5: View of complex **1_4**. The hydrogen-deprived structure of the ligand is made by 117 non-hydrogen atoms with three dandling chains of sp^3 carbons ending with the highest topo-reactive atoms C37,C75,C114.The six atoms with minimum w_i are also represented. The structure of the ligand **4** shows a large distortion of the carbon chains, almost losing the characteristics calixarene cone-shape. The oxygen atoms at the basis of each chain work like atomic hinges and allowing the fluctuation of the chains.

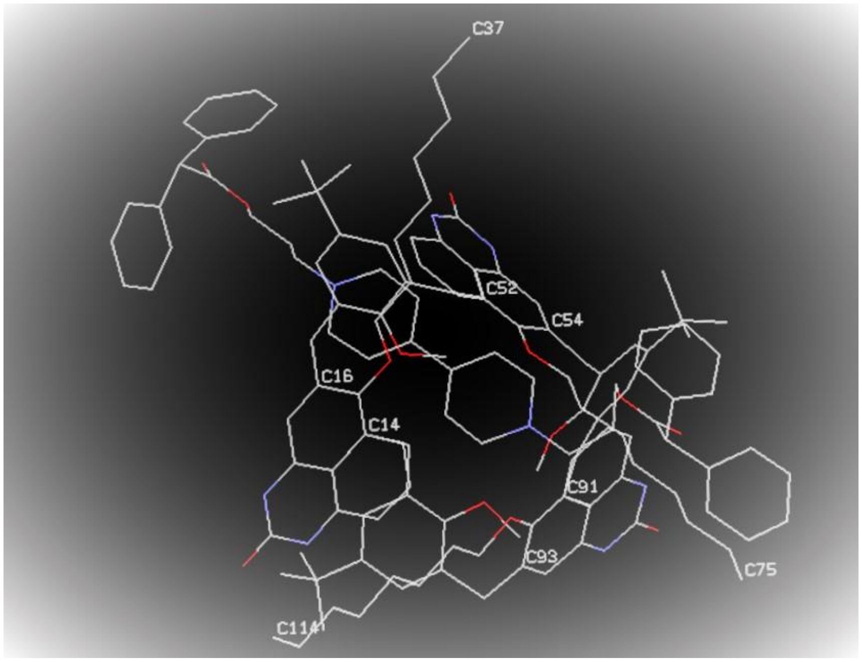

Regarding the relative stability of the three complexes, the simulations of the electronic properties performed in the present paper by quantum computational method are able to rank their relative electronic stability and the one of the preorganised ligand **1, 2, 3 or 4**. It is known from long time [68] that, by assuming the harmonic approximation for the entire crown ether chain, it is possible to estimate for each ligands the energy cost involved in the global deformations in the host-guest complexation process.

In agreement with this finding, the binding studies have shown that **1_4** is indeed the most efficient host-guest complex of the series. The energy values reported in Table 4 have been derived by the mean of original ab-initio computations and they show that ligand of the molecule **3_4** has the most preorganized structure, followed by **2_4** and **3_4**. The last derivative was found to be the least efficient of the remaining stereoisomers, thus indicating that the energy effects resulting by the oriented three carbon chains decrease the stability of the complex.

Another question that present studies pose it is why the ligands in the "partial cone and not those in the alternative conformations" prefer to bind the guest molecule in this series of calix[6]arenes complexes. To this extent, relevant non-bonding interactions are normally to be considered in order to simulate correctly the structural evolutions of the complex.

Topological modelling provides a fast and useful discrimination among these calixarene complexes **1_4, 2_4, 3_4** , the best candidate being the **2_4** system in which the total topological efficiency gets benefited by the complexation with the guest molecule **2,** the rotaxane **2_4,** Table 4 gives a clear overview of the current findings by listing the results of booth simulations, energetical and topological. The starred invariant indicates the **2_4,** as the one with the maximised topological efficiency.

Table 4: Energetic and topological parameters are reported for the host-guest complexes; in both cases the most stable systems are labelled by underscored values.

Rotaxane complex	**Etotal$_{precomplex}$ (kcal/mol)**	**Etotal$_{complex}$ (kcal/mol)**	**Complex topological efficiency (ρ/ρ*)**
1_4	3702346.613	3837167.691	1,0005
2_4	3621720.058	3870660.029	$\underline{1}$
3_4	3477598.596	4045342.867	1,0012

The partial cone structure of the calix[6]arene derivatives seems to represent the best compromise between the stabilizing host-guest interaction and steric (repulsive) contributions. The stability of the **2_4** complex results moreover enhanced by considerations that come from the pure topology of that molecular system. In the present work we have found (see Table 4) the basal correlations between the stability/achievability of the calix[6]arene derivatives and the topological efficiency that represents a measure of a long-range extra symmetry aiming to homogenise the contribution to the Wiener index of every atoms to the one coming from the minimal vertices. The correlation between energetical parameters and topological efficiency has been also listed in the columns tabled and explained. Both these quantities have to be considered for predicting achievable calix[6]arene based structures.

The Wiener index is often used in drug screening because it correlates very well with the physico-chemical characteristics of the compounds (e.g. density, surface tension, van der Waals surface, etc.) but also to predict binding energy in a complex protein-ligand type [69,70]. Rotaxanes are also complexes but of molecular machines type, machines which execute a certain type of movement, movement which implies an exchange of energy between the parts of the complex.

As can be seen both the Etotal$_{complex}$ and the difference, ΔEtotal (Etotal$_{complex}$ - Etotal$_{precomplex}$) correlates very well with the Wiener index, *W*, which suggests a close connection between the total energy of the rotaxanic complex and the compaction of the complex (stabilization degree). The correlation with ΔEtotal being better suggests that at the transition from the precomplex stage to the complex stage, there is a stabilization between the two molecules of the complex due to the interactions and/or the intermolecular forces that are exerted between the two components of the rotaxanic complex, this being more compacted, more stable compared to the precomplex stage. This connection between the stability of the complex and its energy is also reinforced by the fact that Etotal$_{complex}$ and ΔEtotal correlate very well with the extreme topological efficiency index ρ^E, which is also related to the stability of the complex [71]. The starred invariant indicates **2_4,** as the one with the maximized topological efficiency.

From the correlation between the energy ($Etotal_{complex}$, ΔEtotal) and the chemical reactivity indices (χ, η, π, ω) respectively chemical reactivity indices and the topological indices (**ρ, ρ^E**) it can be observed that $Etotal_{complex}$ and ΔEtotal of the rotaxanic molecular complexes with the difference of electronegativity (Δχ) between the complex state and the precomplex state, i.e. with the tendency of the system to transfer electrons. On the second place is the correlation with $\chi_{complex}$, also related with the charge transfer in the rotaxanic complex and the alignment of the middy level of the HOMO-LUMO energy reactivity interval between the two components of rotaxane. It follows correlation with chemical hardness ($\eta_{complex}$), an index that with its maximization principle, expresses the charge transfer during a binding, a transfer that continues until the complex achieves its maximum stability by maximizing the HOMO-LUMO gap so that the next electronic transitions are prevente. For the transition from precomplex to complex stage, it is important the exchange of electrons between the components of rotaxane, respectively the delay of the moment of overcoming the HOMO-LUMO reactivity gap which prevents the final stabilization of rotaxane. This is also confirmed by the fact that $\eta_{complex}$ and Δη correlate very weakly with **ρ, ρ^E** - topological efficiency indices (which indicate topological stability), the delayed maximization of the HOMO-LUMO gap allows continuous load transfer of electrons between the axle and the wheel of the rotaxane, fact that will would allow the execution of the rotation movement.

In the case of the correlations of chemical reactivity indices with **ρ, ρ^E** the best results were obtained for: $\chi_{complex}$, $\pi_{complex}$, Δω. Chemical power and electronegativity involves the transfer of electrons and the alignment of HOMO-LUMO median levels in the complex, these being involve in the topological stabilization of the rotaxanic complex; the difference in electrophilicity highlights the importance of breaking the energy barrier by the ondulatory charge transfer at the transition from the precomplex to the complex stage. This it also can be observe from the hierarchy for *chemical binding scenario* in the case of the **kinetic** complex ($\Delta\omega \rightarrow \Delta\chi \rightarrow \Delta\pi \rightarrow \Delta\eta$), hierarchy realized according to topological efficiency indices (topological stability of the rotaxanic complex). The stabilization of the **kinetic** complex is initiate by the electron ondulatory transfer that crosses the energy barrier between the wheel and the axle of rotaxane. This step is followed by the minimization of the difference of the median levels of the HOMO-LUMO energy reactivity interval between the axle and the wheel, followed by chemical power difference (Δπ) – the transfer of the remaining electron. Final step in this hierarchy is the Δη, variation of chemical hardness, the extension of the HOMO-LUMO interval, the **kinetic** complex remains open for the charge transfer.

In the case of the **stable** complex of molecular machines type / rotaxane type the hierarchy for *chemical binding scenario* is different for the two considerated cases **ρ and ρ^E;** for **ρ** is $\pi \rightarrow \chi \rightarrow \omega \rightarrow \eta$, respectively for **$\rho^E$** is $\chi \rightarrow \omega \rightarrow \pi \rightarrow \eta$. In both cases results a *chemical binding scenario* in which chemical reactivity indices are mixed (first generation: χ, η; second generation: π, ω). In the first case scenario begin with chemical power (π), namely the charge transfer without changing spin, followed by alignment of the middy level of the HOMO-LUMO energy reactivity interval between the two components of rotaxane. In the second case the stabilization of the complex is triggered by electronegativity (χ) and its principle of equalization of the median levels of the energy reactivity interval HOMO-LUMO, continues with one of the indices of the mixed reactivity: the electrophilicity (ω), namely the charge tunneling between the two components of the molecular machine. In both cases the hierarchy is ending with chemical hardness (η) maximizing the HOMO-LUMO energy gap. This particular behavior suggests that we are dealing with a system that remains open until the delayed maximization of the HOMO-LUMO interval, fact that allows the continuous transfer of charge between the components of the rotaxane. This continuous transfer is also necessary in order to be able to perform a translational movement along the axle (or rotating around) of these complexes of molecular machines type, this motion implying a continuous charge transfer between the wheel and axle of the rotaxanic complex.

4. CONCLUSION

On calixare-based rotaxane complexes containing tris(N-phenylureido)-calix[6]arene as wheel and a 4,4'-bipyridinium dication's units as axle we applied topological-chemical reactivity studies (using electronegativity, chemical hardness, chemical power, electrophilicity indices and topological indices like Wiener indice). The results indicate that the most significant structural deformations, which preorganize the molecular structure of the polar cage to allow the formation of the complexes, consist in a geometrical distortion of the chains containing the oxygen atoms. Also it shows a massive preorganisational modifications undertaken by the calixarene to match with its molecular surface the shape of the guest molecule. The binding studies have revealed the most efficient host-guest complex of the serie. The starred invariant indicates the **2_4,** as the one with the maximized topological efficiency. The partial cone structure of the calix[6]arene derivatives seems to represent the best compromise between the stabilizing host-guest interaction and steric (repulsive) contributions. The stability of the **2_4** -complex results moreover enhanced by considerations that come from the pure topology of that molecular system.

From the very good correlation between energies and Wiener index, *W*, it can be concluded that at the transition from the precomplex stage to the complex stage, there is a stabilization between the two molecules of the complex due to the interactions and/or the intermolecular forces that are exerted between the two components of the rotaxanic complex, this being more compacted, more stable compared to the precomplex stage. From the correlation between the energy ($Etotal_{complex}$, ΔEtotal) and the chemical reactivity we conclude that for the transition from precomplex to complex stage, it is important the exchange of electrons between the components of rotaxane, respectively the delay of the moment of overcoming the HOMO-LUMO reactivity gap which prevents the final stabilization of rotaxane.

From the correlations of chemical reactivity indices with $\boldsymbol{\rho}$, $\boldsymbol{\rho^{E}}$ we obtained the hierarchies for *chemical binding scenario* for the **kinetic** complex and the **stable** complex. It can be observed that all these hierarchies starts with the charge transfer without changing spin or charge tunneling followed by alignment of the middy levels of the HOMO-LUMO energy reactivity interval between the two components of rotaxane. All this hierarchies are ending with chemical hardness (η), namely the maximization the HOMO-LUMO energy gap. This behavior indicate that we are dealing with a system that remains open until the delayed maximization of the HOMO-LUMO interval, fact that allows the continuous transfer of charge between the components of the rotaxane. This delayed maximization may be necessary in order to be able to perform a translational movement along the axle (or rotating around) of these complexes of molecular machines type.

ACKNOWLEDGEMENTS

MVP acknowledges his contribution to this work within the Nucleus-Programme under the project PN-19-22-01-02 and its 2020 renewal as funded by the Romanian Ministry of Education and Research. Professors Margherita Venturi from University of Bologna (Italy) and Ioan Neda from Braunschweig Technical University (Germany) are hearty thanked for timely inspirational discussions on molecular machines and on calixarenes structures and properties, respectively.

REFERENCES

1. Desiraju, G. Chemistry beyond the molecule. *Nature* **2001,** *412*, 397–400.
2. Lehn, J.M. Supramolecular chemistry - scope and perspectives molecules, supermolecules and molecular devices. *Angew. Chem. Int. Edn*. **1988,** *27*, 89–112. 10.1002/anie.198800891
3. Stoddart, J.F. The chemistry of the mechanical bond. *Chem. Soc. Rev*. **2009,** *38,* 1802–1820.
4. Stoddart, J.F. Mechanically Interlocked Molecules (MIMs)—Molecular Shuttles, Switches, and Machines (Nobel Lecture) *Angew. Chem. Int. Ed.* **2017**, *56*, 11094 – 11125
5. Steed, J.W.; Atwood, J.L. *Supramolecular Chemistry* 2nd Ed, J. Wiley & Sons: Chichester, UK, 2009.
6. Ariga, K. Supermolecules, In *Biomaterials Nanoarchitectonics*, Ebara M. Eds. Publisher: William Andrew Publishing, NY, SUA, 2016, 25-40.
7. Balzani, V.; Credi, A.; Venturi, M. *Molecular Devices and Machines*; Wiley-VCH Verlag GmbH & Co. KGaA: Weinheim, Germany, 2008.
8. Teo, B.K.; Sun, X.H. From Top-Down to Bottom-Up to Hybrid Nanotechnologies: Road to Nanodevices *J. Clust. Sci.* **2006**, *17* (4), 529–540.
9. James, T.D. Specialty Grand Challenges in Supramolecular Chemistry. *Front Chem*. **2017**, *5*, 83. Published 2017 Oct 17. doi:10.3389/fchem.2017.00083
10. Dudaş, N.A.; Putz, M.V. Chemical reactivity driving switchable molecular machines. A case of Bipyridine -Calixarene rotaxane, *Fuller Nanotub Car N*, **2019,** *27:6*, 514-524, DOI: 10.1080/1536383X.2019.1612379
11. Neal, E.A.; Goldup, S.M. Chemical consequences of mechanical bonding in catenanes and rotaxanes: isomerism, modification, catalysis and molecular machines for synthesis. *Chem Commun (Camb)*. ***2014****; 50(40),* 5128-5142.
12. Bruns, C.J.; Stoddart, J.F, *The Nature of the Mechanical Bond: From Molecules to Machines*, Wiley, New Jersey, SUA, 2016. p.1-90, 271-285.
13. Bruns, C.J.; Stoddart, J.F. Rotaxane-Based Molecular Muscles. *Acc. Chem. Res.*, **2014**, *47(7)*, 2186–2199.
14. Barin, G.; Forgan, R.S.; Stoddart, J.F. Mechanostereochemistry and the mechanical bond. *R. Soc. Lond. Proc. Ser. A Math. Phys. Eng. Sci.*, **2012,** *468*, 2849-2880.
15. McGonigal P.R. Multiply threaded rotaxanes, *Supramol. Chem.*, **2018,** *30(9)*, 782-794.
16. Dudaş, N.A.; Ori, O.; Putz, M.V. Challenging the HSAB principle on molecular machines' precursors. *Fuller Nanotub Car N* (**2021**) 29: 000-000 (in press); DOI: 10.1080/1536383X.2021.1877666.

17. Du, X.-S.; Wang, C.-Y.; Jia, Q.; Deng, R.; Tian, H.-S.; Zhang, H.-Y.; Meguellati, K.; Yang, Y.-W. Pillar[5]arene-based [1]rotaxane: high-yield synthesis, characterization and application in Knoevenagel reaction *Chem. Commun.* **2017**, *53*, 5326–5329.
18. Xu, K.; Nakazono, K.; Takata, T. Design of Rotaxane Catalyst for O-Acylative Asymmetric Desymmetrization of meso-1,2-Diol Utilizing the Cooperative Effect of the Components *Chem. Lett.* **2016**, *45*, 1274–1276.
19. Schalley, C.A.; Beizai, K; Vögtle, F On the Way to Rotaxane-Based Molecular Motors: Studies in Molecular Mobility and Topological Chirality. *Acc. Chem. Res.* **2001,** *34(6)*, 465–476
20. Sauvage, J.P. Transition Metal-Containing Rotaxanes and Catenanes in Motion: Toward Molecular Machines and Motors *Acc. Chem. Res.*, **1998**, *31(10)*, 611–619.
21. Xue, M.; Yang, Y.; Chi, X.; Yan, X.; Huang, F. Development of Pseudorotaxanes and Rotaxanes: From Synthesis to Stimuli-Responsive Motions to Applications *Chem. Rev.* **2015**, *115*, 7398–7501.
22. Venturi, M.; Iorga, M. I.; Putz, M.V. Molecular Devices and Machines: Hybrid Organic-Inorganic Structures *Current Organic Chemistry*, **2017**, *21*, 2731-2759
23. Arduini, A.; Bussolati, R.; Credi, A.; Pochini, A.; Secchi, A.; Silvi, S.; Venturi, M. Rotaxanes with a calix [6] arene wheel and axles of different length. Synthesis, characterization, and photophysical and electrochemical properties. *Tetrahedron*. **2008**; *64(36)*, 8279-8286.
24. Balzani, V.; Credi, A.; Venturi, M. *Molecular Devices and Machines*. *Concepts and Perspectives for the Nanoworld*; Wiley-VCH: Weinheim, Germany, 2008.
25. Monk, P.M.S *The Viologens - Physicochemical Properties Synthesis and application of the salts of 4,4'-Bipyridine*; Wiley: Chichester, UK, 1998.
26. Ballardini, R.; Credi, A.; Gandolfi, M. T.; Giansante, C.; Marconi, G.; Silvi, S.; Venturi, M. Photophysical, photochemical and electrochemical properties of a series of aromatic electron acceptors based on N-heterocycles. *Inorg. Chim. Acta*. **2007**, *360*(3), 1072-1082.
27. Orlandini, G.; Ragazzon, G.; Zanichelli, V.; Degli Esposti, L.; Baroncini, M.; Silvi, S.; Venturi, M.; Credi, A.; Secchi, A.; Arduini, A. Plugging a Bipyridinium Axle into Multichromophoric Calix[6]arene Wheels Bearing Naphthyl Units at Different Rims. *ChemistryOpen*. **2017**; *6(1)*, 64-72.
28. Guérineau, V.; Rollet, M.; Viel, S.; Lepoittevin, B.; Costa, L.; Saint-Aguet, P.; Laurent, R.; Roger, P.; Gigmes, D.; Martini, C.; Huc, V. The synthesis and characterization of giant Calixarenes *Nature Communications* **2019,** *10*, Article number: 113, https://doi.org/10.1038/s41467-018-07751-4
29. Arora, V.; Chawla, H.; Singh, S.P. Calixarenes as Sensor Materials for Recognition and Separation of Metal Ions.*ARKIVOC* **2007**, *ii*, 172-200.
30. Cragg, P.J. *Supramolecular Chemistry: From Biological Inspiration to Biomedical Applications*, **2010**, Springer, USA; p.1-48
31. Gutsche, C D. -Calixarenes: An Introduction, Ed. 2, In *Monographs in Supramolecular Chemistry*, The Royal Society of Chemistry, UK, 2008
32. Agrawal, Y.K., Pancholi, J., Vyas, J.M. Design and synthesis of calixarene. *J SCI IND RES INDIA* **2009,** *68(9)*, 745-768
33. Yang, F.; Guo, H.; Vicens, J. Mini-review: Calixarene liquid crystals. *J. Incl. Phenom. Macrocycl. Chem.* **2014**, *80*, 177–186
34. Da Silva, E.; Ficheux, D.; Coleman, A.W. Anti-thrombotic activity of water-soluble calix[n]arenes. *J. Incl. Phenom. Macrocycl. Chem*. **2005**, *52*, 201–206.
35. Arduini, A.; Ferdani, R.; Pochini, A.; Secchi, A.; Ugozzoli, F. Calix[6]arene as a Wheel for Rotaxane Synthesis *Angew. Chemie*, *Int. Ed.* **2000**, *39*(19), 3453–3456.

36. Arduini, A.; Calzavacca, F.; Pochini, A.; Secchi, A. Unidirectional Threading of Triphenylureidocalix[6]arene-Based Wheels: Oriented Pseudorotaxane Synthesis *Chem. - A Eur. J.* **2003**, *9* (3), 793–799.
37. Arduini, A.; Ciesa, F.; Fragassi, M.; Pochini, A.; Secchi, A. Selective Synthesis of Two Constitutionally Isomeric Oriented Calix[6]arene-Based Rotaxanes *Angew. Chem., Int. Ed.* **2005**, *44*, 278–281.
38. Ugozzoli, F.; Massera, C.; Arduini, A.; Pochini, A.; Secchi, A. Calix [6] arene-based pseudorotaxanes: a solid state structural investigation. *CrystEngComm*, **2004,** *6(39)*, 227-232.
39. Arduini, A.; Bussolati, R.; Credi, A.; Secchi, A.; Silvi, S.; Semeraro, M.; Venturi, M. Toward Directionally Controlled Molecular Motions and Kinetic Intra- and Intermolecular Self-Sorting: Threading Processes of Nonsymmetric Wheel and Axle Components *J.Am. Chem. Soc.* **2013**, *135* (26), 9924–9930.
40. Zanichelli, V., Ragazzon, G., Orlandini, G., Venturi, M., Credi, A., Silvi, S., Arduini, A., & Secchi, A. (**2017**). Efficient active-template synthesis of calix[6]arene-based oriented pseudorotaxanes and rotaxanes. *Organic & biomolecular chemistry, 15 32*, 6753-6763 .
41. Zanichelli, V.; Bazzoni, M.; Arduini, A.; Franchi, P.; Lucarini, M.; Ragazzon, G.; Secchi, A.; Silvi, S. Redox-Switchable Calix[6]arene-Based Isomeric Rotaxanes *Chem. Eur.J* .**2018**, *24*,12370–12382
42. Zanichelli, V.; Dallacasagrande, L.; Arduini, A.; Secchi, A.; Ragazzon, G.; Silvi, S.; Credi, A. Electrochemically Triggered Co-Conformational Switching in a [2]catenane Comprising a Non-Symmetric Calix[6]arene Wheel and a Two-Station Oriented Macrocycle. *Molecules* **2018**, *23*, 1156.
43. Bazzoni, M.; Zanichelli, V.; Casimiro, L.; Massera, C.; Credi, A.; Secchi, A.; Silvi, S.; Arduini, A. New Geometries for Calix[6]arene-Based Rotaxanes, *Eur. J. Org. Chem.*, **2019**, *21*, 3513-3524.
44. Orlandini, G.; Casimiro, L.; Bazzoni, M.; Cogliati, B.; Credi, A.; Lucarini, M.; Silvi, S.; Arduini, A.; Secchi, A. Synthesis and properties of a redox-switchable calix[6]arene-based molecular lasso, *Org. Chem. Front.*, **2020**, doi:10.1039/C9QO01379B
45. Zanichelli, V.; Dallacasagrande, L.; Arduini, A.; Secchi, A.; Ragazzon, G.; Silvi, S.; Credi, A. Electrochemically Triggered Co-Conformational Switching in a [2]catenane Comprising a Non-Symmetric Calix[6]arene Wheel and a Two-Station Oriented Macrocycle. *Molecules*, **2018**, *23*, 1156.
46. Gaeta,C.; Talotta,C.; Neri,P. Calix[6]arene-based atropoisomeric pseudo[2]rotaxanes *Beilstein J. Org. Chem.* **2018,** *14*, 2112–2124. doi:10.3762/bjoc.14.186
47. Putz, M.V.; Dudaş, N.A**.** Variational principles for mechanistic quantitative structure–activity relationship (QSAR) studies: application on uracil derivatives' anti-HIV action. *Struct. Chem.*, **2013**, *24*, 1873.
48. Putz, M.V.; Dudaş, N.A. Determining Chemical Reactivity Driving Biological Activity from SMILES Transformations: The Bonding Mechanism of Anti-HIV Pyrimidines. *Molecules* **2013**, *18*, 9061-9116.
49. Putz, M.V.; Ori, O.; Cataldo, F.; Putz, A.M. Parabolic reactivity <<coloring>> molecular topology. Application on carcinogenic PAHs. *Curr. Org. Chem.* **2013**, *17*, 2816–2830.
50. Putz, M.V.; Putz, A.M. DFT chemical reactivity driven by biological activity: applications for the toxicological fate of chlorinated PAHs. *Struct Bond* **2013,** *150*, 181–232

51. Iczkowski R.P.; Margrave, J.L. Electronegativity. *J Am Chem Soc* **1961,** *83*, 3547–3551
52. Parr, R.G.; Donnelly, R.A.; Levy, M.; Palke, W.E.; Electronegativity: the density functional viewpoint. *J Chem Phys* **1978**, *68*:3801–3808
53. Putz, M.V. Systematic formulation for electronegativity and hardness and their atomic scales within density functional softness theory. *Int J Quantum Chem* **2006,** *106*, 361–389.
54. Putz, M.V.Electronegativity: quantum observable. *Int J Quantum Chem* **2009,** *109*, 733–738
55. Parr, R.G.; Yang, W. *Density-Functional Theory Of Atoms And Molecules*; Oxford University Press: New York, NY, USA, 1989.
56. Putz, M.V.; Russo, N.; Sicilia, E. About the Mulliken electronegativity in DFT. *Theor Chem Acc* **2005,** *114*, 38–45
57. Parr, R.G.; Pearson, R.G. Absolute hardness: companion parameter to absolute electronegativity. *J. Am. Chem. Soc.*, **1983**, *105 (26)*, 7512–7516
58. Pearson, R.G. Absolute electronegativity and absolute hardness of Lewis acids and bases. *J Am Chem Soc* **1985,** *107*, 6801–6806
59. Pearson, R.G. *Chemical hardness*. Wiley-VCH, Weinheim, Germany, 1997.
60. Putz, M.V. *Absolute and chemical electronegativity and hardness*. Nova Science Publishers Inc., New York, USA, 2008
61. Pearson, R.G. *Hard and soft acids and bases*. Dowden, Hutchinson & Ross, Stroudsberg, Germany, 1973
62. Pearson, R.G. Hard and soft acids and bases—the evolution of a chemical concept. *Coord Chem Rev* **1990,** *100*, 403–425
63. a)Putz, M.V.; Tudoran, M.A. Bondonic effects on the topo-reactivity of PAHs. *Int J Chem Model* **2014**, *6(2–3)*, 311–346. b) Putz, M.V.; Ori, O.; De Corato, M.; Putz, A.M.; Benedek, G.; Cataldo, F.; Graovac, A. Introducing “Colored” Molecular Topology by Reactivity Indices of Electronegativity and Chemical Hardness. In: *Topological Modelling of Nanostructures and Extended Systems. Carbon Materials: Chemistry and Physics*, Ashrafi A.; Cataldo F.; Iranmanesh A.; Ori O. Eds., Volume 7, Publisher: Springer, Dordrecht, NL, 2013, pp. 265-287.
64. Ori, O.; Putz, M.V. Topological evolution of the 5|8|5 defect in *graphene New Front. Chem.*,**2018**, *27*(2), 105-113
65. Wiener, H. Structural determination of paraffin boiling points *J. Am. Chem. Soc.*, **1947,** *1(69*), 17–20
66. Devillers, J.; Balaban, A.T. (Eds.) Topological Indices and Related Descriptors in QSAR and QSPR, Publisher: Gordon & Breach, Amsterdam, Holland, 1999.
67. Hypercube, Inc. (**2002**) HyperChem 7.01 [Program Package]; Hypercube, Inc.: Gainesville, FL, USA.
68. Ugozzoli, F.; Ori, O.; Casnati, A.; Pochini, A.; Ungaro, R.; Reinhoudt D.N. Evidence for cation-π interactions in calixcrown·KPic complexes from X-ray crystal structure analysis and energy calculations, *Supramolecular Chemistry,* **1995,** *5:2,* 179-184, DOI: 10.1080/10610279508029492
69. Estrada, E.; Patlewicz, G.; Uriarte, E. From molecular graphs to drugs. A review on the use of topological indices in drug design and discovery. *Indian J. Chem.,* **2003,** *42*, 1315-1329

70. Rouvray, D.H. The rich legacy of half century of the Wiener index, in *Topology in Chemistry: Discrete Mathematics of Molecules*, Rouvray, D.H.; King, R.B.; Eds.; Publisher: Horwoord, Chichester, UK; 2002, pp. 16-37
71. Koorepazan-Moftakhar, F.; R Ashrafi, A.; Ori, O.; Putz, M.V. Topological invariants of nanocones and fullerenes. *Curr. Org. Chem.*, **2015,** *19(3)*, 240-248.

NEW FRONT. CHEM. (2020)
Volume 29, Number 2, pp. 99-108
ISSN 2668-9189; ISSN-L 2393-2171
© West University of Timişoara

Former: Ann. West Univ. Timisoara – Series Chem.
ISSN: 1224-9513

Article

CHEMOMETRICS STUDY OF GERMS PLANT FOR DETERMINING ANTICANCER ACTIVITY

***Alina-Maria Petrescu*[1], *Lauriana–Eunice Zbîrcea*[2], *Maria-Roxana Buzan*[2], *Gianina-Loredana Jucos*[3], *Feng Chen Ifrim*[4], *Gheorghe Ilia*[5], *Virgil Paunescu*[6]**

[1]OncoGen Centre, County Hospital "Pius Branzeu", Blvd. Liviu Rebreanu 156, RO-300736, Timisoara, Romania, alinapetrescu79@gmail.com;
[2]University of Medicine and Pharmacy "Victor Babes", Eftimie Murgu Sq. 2, Timisoara, 300041, Romania, zbircea.lauriana@umft.ro; buzan.roxana@umft.ro
[3]West University of Timisoara, Physics Faculty, Blvd. Vasile Parvan, number 4, 300223,e-mail:gianina_lore93@yahoo.com;
[4]Department of Marketing medical technology, Carol Davila University of Medicine and Pharmacy, Bucharest 020021, Romania; adsm.adsm@yahoo.com
[5]Institute of Chemistry of the Romanian Academy, 24 Mihai Viteazu Bvd. 300223, Timisoara, Romania, ilia@acad-icht.tm.edu.ro; gheilia@yahoo.com;
[6]Department of Immunology, University of Medicine and Pharmacy "Victor Babes", Eftimie Murgu Sq. 2, Timisoara, 300041, Romania; virgilpaunescu@oncogen.com;

ABSTRACT

This project started from the premise that in nature, there are substances capable of preventing the occurrence of cancer, or, at least keeping it in its early stages, by using plant germs. Germs were obtained from Biovita germs machine, like: watercress, unshelled and genetically modified soybeans, hyssop, sage, fennel, amaranth, broccoli, radish, alfalfa, cumin, caraway, rye, wheat, buckwheat, and the next step was to extract the substances from these germs, and analyzed by LS/MS, for the identification of polyphenolic compounds, which are antioxidants, which play a very important role in the prevention of cancer, mainly alpha-linolenic acid, the main source of omega 3 fatty acids, essential for the human body. The process was carried out in several stages, namely: the germination period was 4-5 days, followed by maceration in hydroalcoholic solution with 99% ethyl alcohol, then the decoction and percolation in the system provided with separating funnel, filter and Erlenmayer glass. The antioxidant activity was determined using spectrophotometry (Tecan Sunrise™ – A Reliable Absorbance Reader), using as a calibration sample, ascorbic acid, the absorbance of which was already known from the literature data, namely 600 nm. The presence of riboflavin, at an absorbance of 440 nm, allantoin, 517 nm, quercetin, at an absorbance of 385 nm, choline, at 570 nm, and thiamine at an absorbance of 520 nm, was identified. The calibration curve was obtained based on the values of the concentrations used and the absorbance obtained. The scavering was determined, on the basis of which the antioxidant activity was identified.

1. INTRODUCTION

Cancer is characterized by the rapid growth of abnormal cells and is often linked to oxidative stress. [1] Broccoli is loaded with compounds that are believed to protect against cancer. [2]

Observational studies suggest that the consumption of cruciferous vegetables, including broccoli, is linked to a reduced risk of many cancers, including lung, colorectal, breast, prostate, pancreatic, and gastric cancers [3]. A unique family of plant compounds called isothiocyanates sets cruciferous vegetables apart from other veggies. Studies suggest that isothiocyanates affect liver enzymes, reduce oxidative stress, decrease inflammation, stimulate your immune system, and combat the development and growth of cancer. [4] The main isothiocyanate in broccoli, sulforaphane, acts against the formation of cancer at the molecular level by reducing oxidative stress .[5] Sulforaphane occurs at 20–100 times higher amounts in young broccoli sprouts than in full-grown heads of this vegetable [6]. Though broccoli supplements are also available, they may not contribute an equivalent amount of isothiocyanates and thus may not give the same health benefits as eating whole, fresh broccoli [7].

Bile acids are formed in your liver, stored in your gallbladder, and released into your digestive system whenever you eat fat. [8] Afterward, the bile acids are reabsorbed into your bloodstream and used again. Substances in broccoli bind with bile acids in your gut, increasing their excretion and preventing them from being reused. [9]

This results in the synthesis of new bile acids from cholesterol, reducing total levels of this marker in your body. [10]

Two of the main carotenoids in broccoli, lutein and zeaxanthin, are associated with a decreased risk of age-related eye disorders.[11]Vitamin A deficiency may cause night blindness, which can be reversed with improved vitamin A status. [12]

Broccoli contains beta carotene, which your body converts into vitamin A.

This vegetable may thus boost eyesight in individuals with a low vitamin A intake. [13]

Broccoli is considered a goitrogen, which means that high amounts may harm the thyroid gland in sensitive individuals. Cooking this vegetable on high heat can reduce these effects [14]

Individuals taking the blood thinner warfarin should consult with their healthcare practitioner before increasing their broccoli intake because its high vitamin K1 content may interact with this medication. [15]

All plants and animals produce squalene as a biochemical intermediate, including humans. It occurs in high concentrations in the stomach oil of birds in the order Procellariiformes.[16] Squalene is a natural organic compound originally obtained for commercial purposes primarily from shark liver oil (hence its name, as *Squalus* is a genus of sharks), although plant sources (primarily vegetable oils) are now used as well, including amaranth seed, rice bran, wheat germ, and olives. Yeast cells have been genetically engineered to produce commercially useful quantities of "synthetic" squalane. [17]

Squalene is a hydrocarbon and a triterpene, and is a precursor for synthesis of all plant and animal sterols, including cholesterol and steroid hormones in the human body.[18]

Phosphaturic mesenchymal tumor (PMT) [19] is a rare distinctive mesenchymal neoplasm with heterogeneous but recognizable histologic appearances. It frequently elicits a clinical paraneoplastic syndrome consisting of hypophosphatemic hyperphosphaturic osteomalacia due to increased secretion of FGF23 [20]. The patients typically present with gradual muscular weakness, bone pain, and pathologic fractures. The diagnosis is commonly delayed for years due to the non-specific nature of these symptoms, lack of clinical suspicion, failure to include serum phosphorus levels in routine blood chemistry testing, and difficulty in identifying the responsible tumor. Additionally, these tumors are often missed histologically because of their rarity and morphologic overlap with other mesenchymal neoplasms. [21] Complete excision of the tumor is crucial as it typically resulted in the resolution of the osteomalacia, clinical symptoms, and laboratory abnormalities. Observational studies suggest that the consumption of cruciferous vegetables, including broccoli, is linked to a reduced risk of many cancers, including lung, colorectal, breast, prostate, pancreatic, and gastric cancers [3]. A unique family of plant compounds called isothiocyanates sets cruciferous vegetables apart from other veggies.Studies suggest that isothiocyanates affect liver enzymes, reduce oxidative stress, decrease inflammation, stimulate your immune system, and combat the development and growth of cancer.

2. METHOD

2.1. THEORETICAL MODEL

This method was developed in Oncogen laboratory, for determining antioxidant activity by the bases of the absorbance values, obtained by the UV-VIS analysis. It was used the ethanol extract for *in vitro* antioxidant activities and quantitative determination of bio-active compounds,and was made after next steps:

1. The germination of the seeds / Germination
2. Physical Purity
3. The composition of botanical
4. Humidity
5. Molecular weight
6. Viability
7. The germination energy
8. The control surfaces taken

2.2. Experimental Method/Model

This method is based by the Standard Protocol, from that have used:

2.2.1. Chemicals and basic tools:

2.2.1.1.Ethanol 99,0%

2.2.1.2.Na2SO4 , anhidrous
2.2.1.3.Aluminium oxide with granulation for cromatography
2.2.1.4.DSS
2.2.1.5.NaOH sol.
2.2.1.6.HCl sol.
2.2.1.7.ddH2O
2.2.1.8.DMSO
2.2.1.9.Weighing material
2.2.1.10.Filter material
2.2.1.11.Pasteur pipettes

2.3. Equipment

2.3.1. Digital balance
2.3.2. pHmeter
2.3.3. Sonicator
2.3.4. Vortex
2.3.5. Heating source
2.3.6. Graduated 10ml cylinder
2.3.7. Bath water
2.3.8. Liquid column of cromatography
2.3.9. A solvent in which the sample is very soluble (i.e.: carbon tetrachloride, deuterated methanol, DMSO,or ethanol etc.). *It is prudent to try this out first with ordinary methanol, DMSO etc. to have an idea about the relative volumes required before using the deuterated solvents).*

The pH can also be adjusted up or down with NaOH or HCL to aid dissolution.

Add about 3ml of the sonicate, vortex or shake lightly to dissolve sample (avoid frothing).

Glassware

- Molding conical plug
- Pipetts graduated of glass by different capacities
- glass filter
- 50ml cylindrical

-Coloumns of glass chromatography with a length of about 100 mm, an inner diameter of about 10 mm, cock provided at the inner side and having the lower end tapered to a diameter of mm.
-Capsuls porcelain, 50 ml.
-Germinater BIOVITA G1
-Analytical balance
-Stirrer
-Sonicator or Shaker

2.4. Measurement Materials

-site mesh size 2 mm
-Map medium porosity filter
- Porcelain pestle
-Thermometer
-Glass wool

3. APPLICATION

In the first step it was checks the Material Safety Data Sheet for the compounds. From the literature (THE MERCK INDEX),it was check the standard protocol of this method in vitro. Next it was check the qualitative and quantitative characterization of the seeds, that were puts on the BIOVITA germinator.

The obtain germs and the steps of the process , was showed in the next figures:

FIGUREs 1-9. Types of germs plant from different type of beans,like: Schinduf;Fennel; Sage; Hyssop; Kresse ; Soy; Chia.

It was check the temperature,that can also be adjusted to aid the rapid dissolution of sparingly soluble solutes.

After 4-5 days of the germination,it was continuos with the decoction and percolation process of the obtained germs.

The next step it was to pursued the measurement of the concentration of the desired hydrocarbons compounds absorbed by the plant. Adjust the pH back to 7.0 (6.8 – 7.2) and make total volume to 4.0 ml in the graduated tube, by identification the negative effects. There will be pursued an comparison of the efficiency of desired eight types of plants used, tested, namely (kresse, hyssop, sage,soybean,fennel,chia, amaranthus,schinduf).

3.1. Results

The antioxidant activity was determinated by the absorbance values.The values of the measurement values of the molar concentration (mg/mL) ,were showed in the next table.

Table1. The measurement values of the molar concentration of the kresse germs; hyssop germs; sage germs; soy germs; amaranthus germs; chia germs; fennel germs and schinduf germs. The absorbance obtained values are showed in this table.

Type of germs plant of beans	Molar Concentration (mg/mL)										Absorbance (nm)		
											Name of		
											Reference	Antioxidant substance present in germs	
Kresse	0.1179	0.05	0.1332	0.0567	0.0396	0.0464	0.1431	0.0518	**0.1406**	**0.0449**	**Ascorbic acid 518**	**Quercetine**	**385**
Hyssop	0.049	0.051	0.0565	0.0464	0.0506	0.0458	0.0464	0.0461	**0.0461**	**0.0486**		**Hysopine**	**280**
Sage	0.047	0.0463	0.0451	0.047	0.0473	0.0505	0.0431	0.0472	**0.0485**	**0.048**		**Hystamine**	**506**
Soy	0.0452	0.9608	0.0499	0.7696	0.0495	0.3669	0.0456	0.4933	**0.046**	**0.5299**		**Flavin**	**440**
Amaranthus	0.2442	0.2102	0.1971	0.1925	0.285	0.1416	0.2051	0.2194	**0.2396**	**0.2536**		**Choline**	**570**
Chia	0.2485	0.3316	0.3289	0.3685	0.3139	0.3192	0.3484	0.2498	**0.2918**	**0.2519**		**Cyannine**	**694**
Fennel	0.2971	0.3109	0.2432	0.3466	0.2284	0.2669	0.2597	0.2835	**0.2379**	**0.2556**		**Tanin**	**760**
Schinduf	0.1068	0.1159	0.1115	0.1114	0.1046	0.1202	0.0925	0.0964	**0.0734**	**0.0932**		**Quercetine**	**385**

3.2. Discussion

The scavering was calculated by the plot of the concentration values, by the obtained absorbance values (nm). The next figures are:

1. The plot of the creson(kresse) concentration, besides of the absorbance values (Figure 10);
2. The plot of the hyssop concentration, besides of the absorbance values (Figure 11);
3. The plot of the sage concentration, besides of the absorbance values (Figure 12).
4. The plot of the soy concentration/ by absorbance values by the absorbance values (Figure 13).

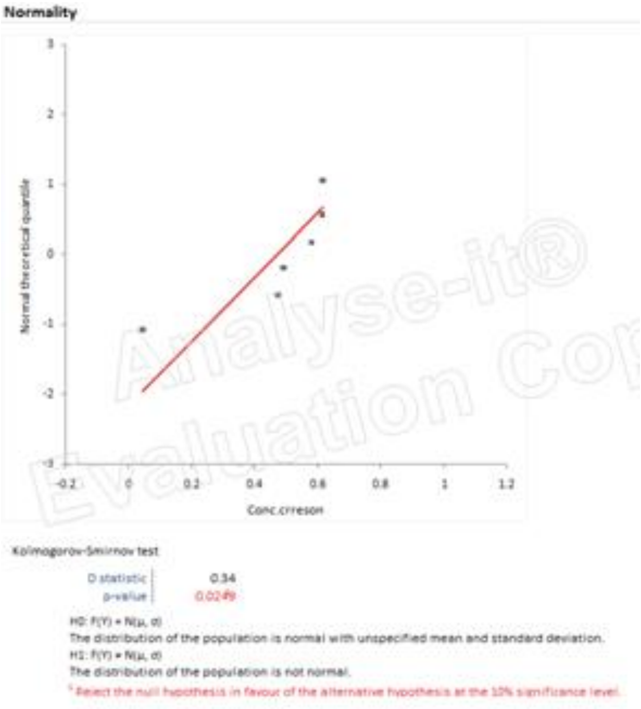

Kolmogorov-Smirnov test

D statistic	0.34
p-value	0.0249

H0: F(Y) = N(μ, σ)
The distribution of the population is normal with unspecified mean and standard deviation.
H1: F(Y) ≠ N(μ, σ)
The distribution of the population is not normal.
* Reject the null hypothesis in favour of the alternative hypothesis at the 10% significance level.

Figure 10.The plot of the c_{creson}(kresse) concentration

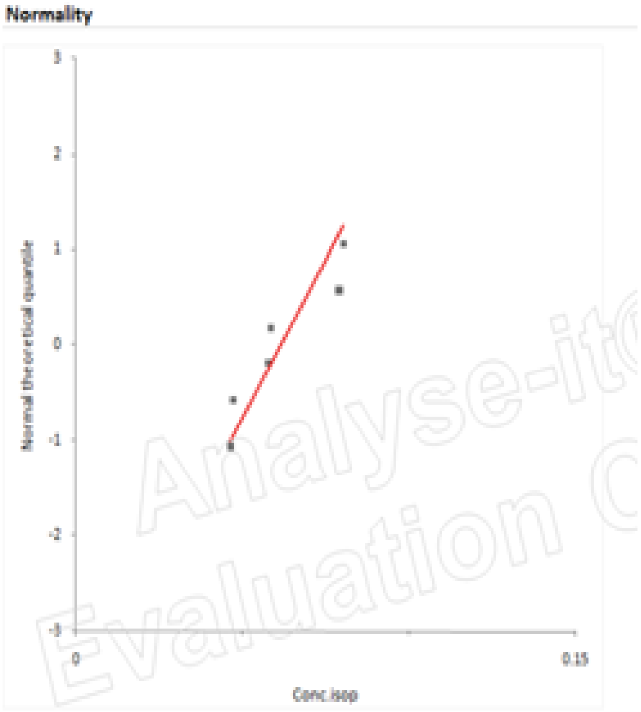

Figure11.The plot of the $c_{\text{hyssop(mg/mL)/Abso}}$

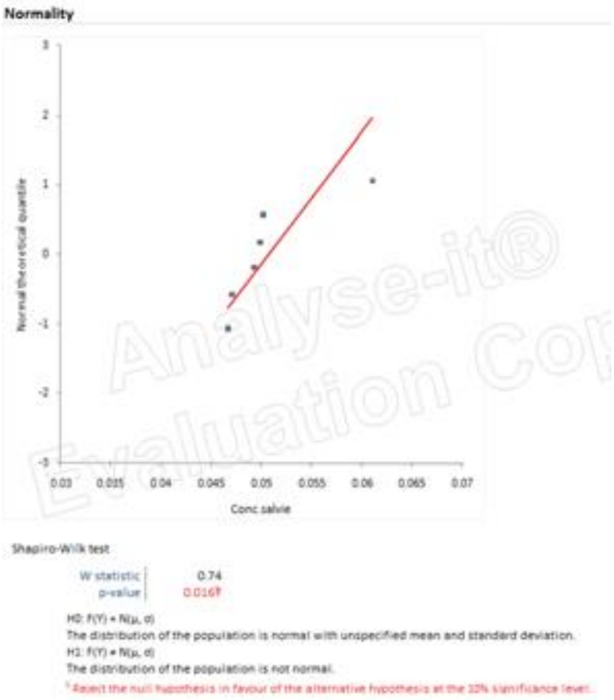

Shapiro-Wilk test

W statistic	0.74
p-value	0.016†

H0: F(Y) = N(μ, σ)
The distribution of the population is normal with unspecified mean and standard deviation.
H1: F(Y) ≠ N(μ, σ)
The distribution of the population is not normal.
† Reject the null hypothesis in favour of the alternative hypothesis at the 10% significance level.

Figure12. The plot of the c_{sage} (sage)concentration/absorbance values

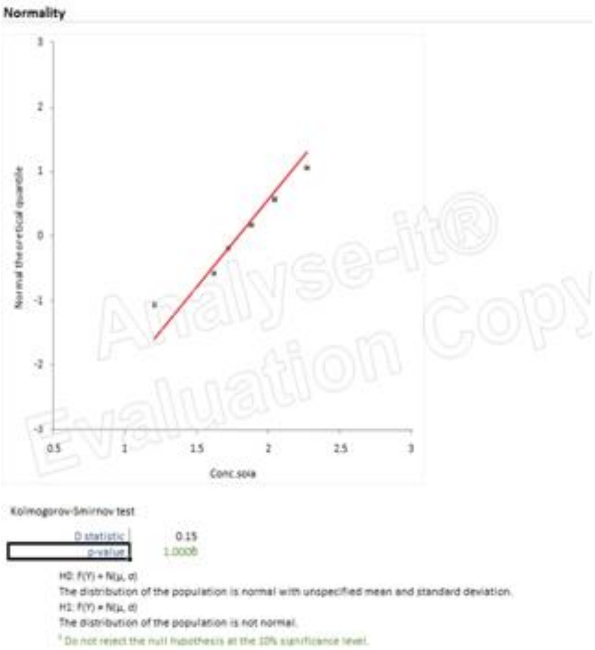

Kolmogorov-Smirnov test

D statistic	0.15
p-value	1.000†

H0: F(Y) = N(μ, σ)
The distribution of the population is normal with unspecified mean and standard deviation.
H1: F(Y) ≠ N(μ, σ)
The distribution of the population is not normal.
† Do not reject the null hypothesis at the 10% significance level.

Figure 13. The plot of the $c_{\text{soy concentration/ by absorbance}}$ values

4. CONCLUSION

In this paper, we are used a series of hydroalchools extracts, with different concentrations, by 15ml, 25ml, 50ml si 75ml, with 99.0% ethanol. The germs were obtained by different plants like: broccoli, kresse, Hyssop, Sage, Soy, Amaranthus, Chia, Fennel and Schinduf. In this UV-VIS analyse,for identify the absorbances, we are obtain : Quercetine , (A= 385 nm); Hyssopina, (A= 280 nm), Hystamine (A=506 nm), Phlavine (A=440nm), Choline (A=570nm), Cyannine (A=694nm), Tannin (A=760nm).

ACKNOWLEDGEMENT

The research was supported by PROJECTS PN-II-PD -2019.

REFERENCES

1. Mitsiogianni, M.; Koutsidis, G.; Mavroudis, N.; Trafalis, T.D.; Botaitis, S.; Franco,R.; Zoumpourlis,V.; Amery,T.;Galanis, A.; Pappa, A.; Panayiotidis,I.M. The Role of Isothiocyanates as Cancer Chemo-Preventive, Chemo-Therapeutic and Anti-Melanoma Agents. *Antioxidants* (Basel); **2019**,8(4): 106;
2. Sestili,P.; Fimognari, Carmela. Cytotoxic and Antitumor Activity of Sulforaphane:The Role of Reactive Oxygen Species. *Biomed Research Int*ernational; **2015**,402386;
3. Wang, H.; Khor,O. T.;Shu, L.; Zhengyuen Su, Francisco Fuentes, Jong-Hun Lee, and Ah-Ng Tony Kong. Plants Againsts Cancer:A Review on Natural Phytochemicals in Preventing and Treating Cancers and Their Druggability. *Anticancer Agents in Medicinal Chemistry*; **2012**;12(10): 1281–1305;
4. Leng, C.; Zhang, Y.; Wang Pei, M.; Zhenxin,W.; RunqiangYang,G. Dynamic variation of glucosinolates and isothiocyanates in broccoli sprouts during hydrolysis. *Scientia Horticulturae*, **2019**,255, pp: 128-133;
5. Wei,L; **Liu** ,C.**;** Zheng, H.; Zheng, L**.** Melatonin treatment affects the glucoraphanin-sulforaphane system in postharvest fresh-cut broccoli (*Brassica oleracea* L.) *Food Chemistry*,**2020**,307, 125562**;**
6. Brasil, M.I.; WasimSiddiqui, M. Preharvest Modulation of Postharvest Fruit and Vegetable Quality, **2018**, pp: 1-40, Chapter 1 - Postharvest Quality of Fruits and Vegetables: An Overview,
7. Marcus B.Jacqueline. Chapter 6 - Lipids Basics: Fats and Oils in Foods and Health: Healthy Lipid Choices, Roles and Applications in Nutrition, Food Science and the Culinary Arts, The Science and Practice of Healthy Cooking,Culinary Nutrition, **2013**, pp: 231-277;
8. Jacobson, A.; Maki, C.K. ; Orringer, E.C.; Jones, H.P. ; Kris-Etherton, P.; Sikand, G. h La Forge,R.; Daniels, R.S.; Wilson, P.D; Morris, B.P. ;Wild, R. A.; Grundy, M.S.; Daviglus, M.; Keith C.F.; Vijayaraghavan, K.; Deedwania C.P.; Aberg, A. J.; Liao, P.K., Brown, V. Recommendations for Patient-Centered Management of Dyslipidemia: Part 2, Journal of Clinical Lipidology. National Lipid Association Recommendations – Part2,**2015,** 9,(6), Supplement, , pp: S1-S122.e1;

9. Hulley, B.S. American Journal of Obstetrics and Gynecology, A national program for lowering high blood cholesterol, **1988**, 158,(6), Part 2, pp: 1561-1566;
10. Bernstein, S. ; Li, B. ; Vachali, P. ; Gorusupudi,A.; Shyam, R., Henriksen,S.; Nolan, M. J.Lutein, zeaxanthin, and *meso*-zeaxanthin: The basic and clinical science underlying carotenoid-based nutritional interventions against ocular disease. Progress in Retinal and Eye Research, **2016,**50,pp: 34-66;
11. Chiu, H.F.; Shen, Y.C.; Venkatakrishnan K.; Wang,C.K. Food for Eye Health: Carotenoids and Omega-3 Fatty Acids, Encyclopedia of Food Chemistry, **2019**, pp: 313-322;
12. Marcus, B.J. Chapter 7 **-** Vitamin and Mineral Basics: The ABCs of Healthy Foods and Beverages, Including Phytonutrients and Functional Foods: Healthy Vitamin and Mineral Choices, Roles and Applications in Nutrition, Food Science and the Culinary Arts,Culinary Nutrition.The Science and Practice of Healthy Cooking, **2013**, pp: 279-331;
13. Gardner, T.;Vazquez, R. S.; Kim, K.; Jones, E.A.; Witt, M. D. Providers' utilization and perceptions of warfarin dosing algorithms, Thrombosis Research, **2019,**183, pp: 4-12;
14. Dorakumbura, N.B.; Busetti, F.; Lewis, W. S. Analysis of squalene and its transformation by-products in latent finger marks by ultrahigh-performance liquid chromatography-high resolution accurate mass Orbitrap™ mass spectrometry, Forensic Chemistry, **2020**,17,100193;
15. Adlington, K.; El harfi, J.; Li, J.; Carmichael, K.; Guderian, J. A.; Fox, C. B.; Irvine, D. J. Molecular Design of Squalene/Squalane Countertypes via the Controlled Oligomerization of Isoprene and Evaluation of Vaccine Adjuvant Applications. Biomacromolecules, 17(1), 165–172, 2015;
16. Heller,J.H;Heller, M.S.;Springer S.; Clark ,E.; Squalene Content of Various Shark Livers. *Nature*; **1957**;179, pp:919–920;
17. Stidworthy, F.M.; Denk,D. Chapter 27 **-** Sphenisciformes, Gaviiformes, Podicipediformes, Procellariiformes, and Pelecaniformes, Pathology of Wildlife and Zoo Animals, **2018**, pp: 653-684, 684.e1, 685-686;
18. Nyström,L.; Whitaker, D. B. ;Winkler-Moser, K.J.; Baer, J.D., Gebauer, K.S.; Hicks, B.K.Phytosterols and their derivatives: Structural diversity, distribution, metabolism, analysis, and health-promoting uses, Progress in Lipid Research, **2018**,70, pp: 35-61;
19. Folpe, L. A. Phosphaturic mesenchymal tumors: A review and update. Seminars in Diagnostic Pathology ,**2019**, 36, (4), 2019, pp: 260-268;
20. Pastor Arroyo, E.M.; Gehring, N.; Krudewig, C.; Costantino, S.; Bettoni, C.; Knöpfel, T.; Sabrautzki, S.; Lorenz-Depiereux, B.; Strom, M.T.; Hrabě de Angelis, M.; Camici, G. G.; Paneni,F.;Wagner, C.A.;Rubio-Aliaga, I. The elevation of circulating fibroblast growth factor 23 without kidney disease does not increase cardiovascular disease risk, Kidney International, 2**018,** 94, (1), pp:49-59;
21. Hatfield, B.S.; Mochel, M. C.; Smith, S.C. Mesenchymal Neoplasms of the Genitourinary System: A Selected Review with Recent Advances in Clinical, Diagnostic, and Molecular Findings, Surgical Pathology Clinics, **2018,**11,(4),pp: 837-876.